2018

Emissions of fine particulate matter from tropical peat fires

Christopher Thomas Roulston
University of Wollongong

UNIVERSITY OF WOLLONGONG AUSTRALIA

Emissions of fine particulate matter from tropical peat fires

Christopher Thomas Roulston

Supervisor:

Dr. Clare Murphy (Dr. Clare Paton-Walsh)

This thesis is presented as part of the requirement for the conferral of the degree:

Masters of Philosophy – Chemistry

This research has been conducted with the support of the Australian Government Research Training Program Scholarship

The University of Wollongong

School of Chemistry

February 2018

- Blank Page -

Certification

I, Christopher Thomas Roulston, declare that this thesis submitted in fulfilment of the requirements for the conferral of the degree Masters of Philosophy – Chemistry, from the University of Wollongong, is wholly my own work unless otherwise referenced or acknowledged. This document has not been submitted for qualifications at any other academic institution.

_____

Christopher Thomas Roulston

15 of February 2018

Abstract

This thesis describes the work undertaken to determine the rate at which particulates are emitted from tropical peat fires in peninsula Malaysia. The emission of particulate matter (PM) during wild fire events around the world contributes to many negative effects on both communities in the local vicinity and (through transport mechanisms) other locations around the globe. These negative effects include; pre-mature mortality, decreased lung function and quality of life, and a decrease in yields from crops in farming regions due to aerosol loading. Despite all of these ill effects, very little is known about the particulate emissions from tropical peat fires. This thesis aims to address some of the knowledge gaps within current research.

There are three main components to this thesis. The first describes a weeklong study hosted at the Victoria University, Werribee campus. This study compared numerous particulate-matter measuring instruments within a smoke chamber. The study was conducted by introducing wood smoke, coal smoke and diesel exhaust into the chamber, which was mixed and held at predefined concentrations before being allowed to return to background levels. The Office of Environment and Heritage (OEH), Lidcombe, NSW, provided; an Aurora 1000G Ecotech Nephelometer, a Thermo Scientific Model 48i Gas Filtration CO Analyser and a DustTrak-DRX 8533 aerosol monitor to be used for this Masters research. The smoke chamber study provided evidence that the instrumentation to be deployed on further field studies through this project provided accurate and precise results (within the estimated uncertainties) when compared to a gravimetric standard.

The second part of this thesis describes the initial Malaysian field campaign. This campaign focused on peat fires in peninsula Malaysia, measuring the levels of carbon monoxide (CO) and PM with an aerodynamic diameter less than or equal to two and a half microns ($PM_{2.5}$), within the smoke plumes from the fires. The emission factor of CO was determined using an open path MIDAC FTIR (Fourier Transform Infrared) spectrometer operated by Thomas E. L. Smith from Kings' College London. The ratio between $PM_{2.5}$ and CO measured in the smoke plume was multiplied by the emission factor for CO to determine an emission factor for $PM_{2.5}$. The results from this study showed a trend not previously observed in the field, that as a peat fire ages the emission ratio of $PM_{2.5}$ decreases. This anti-correlation between age and levels of $PM_{2.5}$ released, provided the basis for a new hypothesis: as the peat fire progresses below the surface, an increasingly deep ash layer is formed, which filters $PM_{2.5}$ from the smoke, thus lowering the emission ratio of $PM_{2.5.}$

The third section of this thesis was an expansion of the second study, where a laboratory study was conducted to provide further evidence to test the hypothesis from the previous campaign. This study used peat that had been sourced from the same fields as the initial campaign. It was then dried and bulk density measured to ensure consistency between samples. Three laboratory burns were undertaken in total, each lasting in excess of 40 hours. The fires were ignited using nichrome wrapped around a ceramic plate that had a charge run through it to generate a flameless

ignition. In the first two burns the fire could progress normally for many hours, and then (when particulate emissions had declined substantially) the layer of ash was carefully removed from the surface and the fire allowed to progress once more. The third burn was an ash addition experimental fire: about an hour after the ignition of the burn, a layer of pre-incinerated ash was added across the surface of the burning peat. Samples from this ash layer were taken at different depths and stages of the burn and tested to examine the carbon content. If the carbon content of the ash increased as the burn progressed, this would be further evidence that the ash layer was a sink for the missing $PM_{2.5}$ from the measured emissions. The results from these burns confirmed the hypothesis that as fires burn the $PM_{2.5}$ emissions reduce despite the combustion efficiency remaining stable. The ash addition experiment yielded positive (although not statistically definitive) results showing an increase in percentage carbon after the conclusion of the burn.

The results from this Masters thesis provide additional knowledge about the nature of peat fires and their emissions of PM. The findings can be used within fire emissions inventories and coupled with chemical transport models, to better understand the effects that large scale tropical peat fires can have on regional air quality and climate.

Acknowledgements

I would like to acknowledge the support provided by my family during this Masters project, in providing a place to stay and store my things in between all the field work trips and in assistance with travelling. I would like to thank my father (Mervyn Roulston) and Aaron Williams for helping with the construction of the smoke sampling hood during their Christmas breaks from work.

I would like to thank Dr, Clare Murphy (Dr. Clare Paton-Walsh) from the University of Wollongong, for supervising me during this project, providing me with guidance and expertise throughout the course, including decisions on the topic and which avenues and opportunities to follow. I also want to thank her for providing assistance during every field campaign; travelling with me to help with initial setup and preparation of the field equipment in Malaysia; her support during my bout of food poisoning whilst overseas; providing editing assistance in writing my thesis and giving me the pushes I needed to get through the project as a whole.

I would like to thank John Kirkwood and Gunarataban Gunachanhar for their assistance in providing instrumentation on loan from the Office of Environment and Heritage, Lidcombe, NSW; and their help in deciding appropriate instrumentation to use and in providing training. I also thank Joseph Ho from the NSW OEH, for technical assistance and conducting the calibrations of instrumentation before and after field campaigns. I also thank John Kirkwood, Matthew Riley and the rest of the NSW OEH for providing opportunities like this to myself and other students.

Invaluable assistance was provided abroad by Dr. Thomas E. L. Smith, including local knowledge and expertise, additional instrumentation, assistance in research and advice about writing techniques and friendship supporting me while conducting field research in a foreign country.

I thank Dr. Elise Andrée-Guerette from the University of Wollongong, for her support during the Werribee smoke chamber campaign and for providing her expertise in data processing, interpretation and display throughout my entire Masters research.

I thank Dr. Stephanie Evers for providing expertise and additional instrumentation, in the form of percentage carbon and nitrogen analysis of sampled ash and also for providing local knowledge, friendship and entertainment between fieldwork days.

I thank Dr. Catherine Yule for providing access to the Monash University, Sunway Bangsar Campus, Malaysia; allowing the use of instrumentation and technical staff assistance. Also, thanks for allowing us to conduct laboratory burns on her back porch - sorry about the excess smoke during testing!!

I thank Jessa H. Thurman from Monash University, Sunway Bangsar Campus, Malaysia, for completing the final stages of fuel moisture and bulk density testing after I needed to leave Malaysia due to severe food poisoning.

Finally I would like to thank the entire University of Wollongong, Center for Atmospheric Chemistry team and in particular Dr. Jenny Fisher for helping me to find

an interest in atmospheric chemistry and providing and entrance to this amazing group; Travis Naylor for his technical expertise and assistance with logistics and Dr. Stephen Wilson for his assistance throughout and after my Masters project.

List of Abbreviations

Acronym	*Expansion*
AQI	Air Quality Index (A metric for simplifying and summarising negative air quality indicators into a single number for the general public)
CAC	Centre for Atmospheric Chemistry
CFA	Country Fire Authority (Victorian volunteer fire fighters)
CO	Carbon Monoxide
CO_2	Carbon Dioxide
COHb	Carboxyhaemoglobin
EPA	Environmental Protection Agency
FTIR	Fourier Transform Infrared
Hb	Haemoglobin
HCN	Hydrogen Cyanide
HR	Hazard Reduction (Controlled fire for the reducing natural fuel loads)
NH_3	Ammonia
NO	Nitric Oxide
NO_2	Nitrous Oxide
NOx	Oxides of Nitrogen (encompasses NO and NO_2)
NSW	New South Wales
PM	Airborne Particulate Matter
$PM_{2.5}$	Particulate Matter less than 2.5 micrometres in diameter
PM_{10}	Particulate Matter less than 10 micrometres in diameter
RFS	Rural Fire Service (New South Wales volunteer fire fighters)
RP	Respirable Particles
STEL	Short Term Exposure Limit (15 min)
TWA	Time Weighted Average exposure limit (8 hours)
Vic	Victoria

Table of Contents

List of Tables, Figures and Illustrations

Chapter 1: Introduction

1.1 Biomass burning emissions and impacts

The term "biomass burning" encompasses prescribed burns, wild fires, and biofuel usage [*Langmann et al.*, 2009]. For the purpose of this thesis, biofuels are excluded unless otherwise stated. The effect of emissions from biomass burning extends from a global impact [*Akimoto*, 2003; *Langmann et al.*, 2009], to local air quality [*Davies and Unam*, 1999; *Haikerwal et al.*, 2015; *Kunii et al.*, 2002; *Vedal and Dutton*, 2006] and individual health [*Ezzati and Kammen*, 2001; *Johnston et al.*, 2011; *Kunii et al.*, 2002; *Reisen et al.*, 2015; *Reisen et al.*, 2011], and has been extensively researched across numerous campaigns. It has been estimated that the majority of wildfires are ignited as a result of human activities (including sparks from railroad engines, cigarettes and intentional ignition), while only a small percentage are started by lightning [*Andreae*, 1991]. Historically, intentional lighting has been used to clear agricultural land, in hunting and for religious or cultural reasons. These are evident through historical records and by the abundance of specific species of plants and the absence of others [*Andreae*, 1991; *Yibarbuk et al.*, 2001].

Emissions from biomass burning

Under the ideal conditions of complete combustion, biomass burning would produce carbon dioxide (CO_2) and water vapour (H_2O). Although complete combustion is unachievable under standard conditions, the dominant fraction of carbon released from vegetation fires is identified as being 90-95% CO_2 and CO [*Akagi et al.*, 2011]. Additional trace level carbon species emitted due to incomplete combustion include; methane (CH_4), particulate matter (PM), aldehydes and numerous other trace gases [*Levine et al.*, 1993]. On a global scale, emissions of these trace species have a significant effect on atmospheric concentrations, with biomass burning emissions rivalling fossil fuel combustion emissions in magnitude [*Crutzen and Andreae*, 1990]. Due to long-range transport of these emissions, fires in one location could affect large areas of the world [*Andreae*, 1983; *Fishman et al.*, 1991]. Tropical peatland fires release enormous amounts of carbon into the atmosphere in various forms [*Page et al.*, 2002; *Turetsky et al.*, 2015], and are estimated to account for more than 25% of the global total greenhouse gas (GHG) emissions from deforestation and forest degradation [*Ballhorn et al.*, 2009; *Van der Werf et al.*, 2010]. Additionally these fires are destroying unique and irreplaceable ecosystems, which currently have unmeasured or unpublished effects on the greater ecosystems surrounding them.

Emission factors

An emission factor (EF_i) is the mass of a gaseous species (i) emitted per unit of dry fuel consumed, generally expressed in $g.kg^{-1}$. EF_i for trace gases of interest can be calculated using [*Ward and Radke*, 1993]:

$$EF_i = F_c \times 1000 \times \frac{MM_i}{12} \times \frac{C_i}{C_T}$$

Equation 1 Emission Factor of species *i*

as used previously by [*Ward and Radke*, 1993], where EF_i is the mass in grams of species *i* emitted per kilogram of dry fuel burned, ($g.kg^{-1}$). F_c is the fractional carbon content of the fuel, MMi is the molecular mass of species *i*, with 12 being the atomic mass of carbon; C_i/C_T is the number of moles of species *i* emitted divided by the total number of moles of carbon emitted, and may be calculated directly from excess mole fractions according to Equation 2.

$$\frac{C_i}{C_T} = \frac{\Delta[i]}{\sum_{j=1}^{n}(NC_j \times \Delta[j])}$$

Equation 2 Number of moles of species *i*

where Δ[i] and Δ[j] are the excess mole fractions of species *i* and *j* respectively (e.g. [*i*] measured in the smoke, minus the mean background mole fraction measured in a nearby locale not affected by smoke $[i]_{bkgnd}$, or if wind direction is recorded wind measured from a clean sector is also viable), NC_j is the number of carbon atoms in compound *j* and the sum of all carbon containing species emitted by the fire[1]. Ninety to ninety-five percent of emitted carbon from biomass burning is in the form of CO_2 and CO, the remaining as CH_4, other VOCs and PM [*Akagi et al.*, 2011]. Yokelson estimates the use of only those carbonaceous species detected by Open Path Fourier transform spectrometry in this mass balance Equation, artificially inflates emission factors by only 1-2% and this error is small compared with other uncertainties inherent in the technique [*Yokelson et al.*, 2007].

C_i/C_T may also be calculated using emissions ratios with respect to a reference species (for example determining emission factors for PM using a known emission factor of carbon monoxide (EF_{CO}) throughout this campaign) via Equations 3 and 4:

$$\frac{C_i}{C_T} = \frac{ER_{i/y}}{\sum_{j=1}^{n}(NC_j \times ER_{j/y})}$$

Equation 3 Emitted moles of species *i* using emission ratio of *i* and *y*

[1] In this study, a wide variety of carbonaceous species were retrieved using the MIDAC OP-FTIR (CO_2, CO, CH_4, C_2H_2, C_2H_4, C_2H_6, H_2CO, CH_3OH, HCOOH and CH_3COOH) to calculate the mole fraction of CO that is used in determining EF_i in Equation 1. Whilst this is not a complete representation of all carbon-containing species emitted by fires, they account of a vast majority (~>98%).

where $ER_{i/y}$ is the emission ration of species *i* (PM) to the reference species *y* (CO) given by:

$$ER_{i/y} = \frac{\Delta[i]}{\Delta[y]} = \frac{[i] - [i]_{bkgnd}}{[y] - [y]_{bkgnd}}$$

Equation 4 Emission ratio of *i* and *y*

where $\Delta[i]$ is the excess mole fraction of species *i*.

Emission ratios may also be determined via the gradient of a well correlated line of best fit to a plot of abundance of species *i* against abundance of known reference species *y*, removing the requirement for accurate knowledge of background mole fractions, while introducing an insignificant degree of error [*Wooster et al.*, 2011].

An emission factor of one species may be calculated via the emission ratio to a reference species with known emission factor via Equation 5:

$$EF_x = \frac{\Delta x}{\Delta i} \times EF_i$$

Equation 5 Emission factor of x determined using an emission ratio and a known emission factor.

Historically the fraction of carbon emitted as PM is omitted from gaseous emission factor determination because it was considered negligible [*Wooster et al.*, 2011]. However, a recent study of PM emission factors from tropical peatland fires suggested that the levels of PM emitted are not negligible in magnitude. Hence it is suggested that for peat fires, these emissions are accounted for in determining the gaseous emission factors (Equation 6) [*Jayarathne et al.*, 2016]. Using a modified version of Equation 1 particulate emissions can be accounted for when determining gaseous emission factors:

$$EF_{CO} = (F_C - F_{PMC}) \times 1000 \times \frac{MM_{CO}}{AM_C} \times \frac{\Delta_{CO}}{\sum_{i=1}^{n}(NC_i \times \Delta_i)}$$

Equation 6 Emission factor of CO accounting for PM emissions

where; EF_{CO} is the emission factor of CO, F_c is measured carbon mass fraction of the fuel, F_{PMC} is the fraction of carbon released as PM, MM_{CO} is the molecular mass of CO (28.01 $g.mol^{-1}$), AM_c is the atomic mass of carbon (12 $g.mol^{-1}$), Δ_{CO} is the excess CO above background, NC_i is the number of carbon atoms in species *i*, Δi is the excess of species *i* above background [*Smith et al.*, 2017].

Finally, the intensity of a fire is determined by its combustion efficiency. An easily measurable approximation of this is given by [*Hao and Ward*, 1993] through the use of a modified combustion efficiency (MCE). MCE gives an approximation of combustion efficiency by estimating the amount of carbon emitted as CO_2:

$$MCE = \frac{\Delta \mathrm{CO}_2}{\Delta CO_2 + \Delta CO}$$

Equation 7 modified combustion efficiency (MCE)

Equation 7 requires a measurement of background mole fraction of CO_2 and CO to accurately estimate ΔCO_2 and ΔCO. ΔCO_2 is the concentration of CO_2 above background levels and ΔCO is the concentration of CO above background. MCE allows the comparison of similar burns and can provide evidence that emission factors generated from separate burns are comparable by showing they are burning with similar efficiencies.

When measurements are conducted significantly downwind of a fire, the smoke has chemically aged before it is sampled. Ratios derived from this aged smoke are referred to as "enhancement ratios", highlighting the chemical and physical processes, which may have altered the ratio of species originally emitted from combustion.

1.2 Air Quality Effects of Smoke from Biomass Burning

Emissions from biomass burning have significant impact on local air quality and hence the health of anyone in the local vicinity of these emissions. Adverse health effects from high trace gas and particulate levels can range from short-term minor irritation of the eyes, shortness of breath and reduced cognitive functions, to longer lasting issues such as impaired respiratory function, memory loss and increased risks of cancer [*Raub et al.*, 2000; *Reisen and Brown*, 2009]. These can affect those in the immediate area of a burn (such as firefighters), and can have a significant impact on the air quality in downwind areas including towns and urban centers.

Adverse health effects from biomass burning emissions are primarily caused by a local increase in trace gases and elevated levels of PM. PM may have other toxins adsorbed to the surface, increasing the health impacts [*Reisen and Brown*, 2009].

Tropical peatland fires almost exclusively smoulder with little to no burning occurring in the flaming stage. Due to this, the levels of carbon monoxide, PM and trace toxins produced per kilogram of fuel burnt is often much higher than that of flame dominant fires. Also, unlike forest fires, which burn with high intensity short-lived burns, lofting emissions high into the atmosphere, the lower temperature peat smouldering typically burns for a much longer time, with emissions generally becoming trapped within the planetary boundary layer. An example of this was during the 2015 Asian haze event [*Field et al.*, 2016], when fires across the region carpeted much of Asia with a long lasting plume of toxins from September through October [*Huijnen et al.*, 2016]. This type of event shows how long-range transport of emissions from fires can affect large areas of the world despite being sourced from a single location or incident [*Andreae*, 1983; *Edwards et al.*, 2006; *Viatte et al.*, 2015].

Carbon Monoxide (CO)

Carbon monoxide (CO) is produced through incomplete combustion and is therefore particularly prominent in the smouldering phase of burns. Given that the length of the smouldering phase is generally much greater than the flaming phase, CO is a major pollutant produced by fires and the health effects of CO are of particular interest. CO is a highly toxic gas with numerous documented and studied health effects.

The primary negative health effects of CO stem from its affinity to haemoglobin (Hb) being more than two hundred times higher than that of oxygen (O_2) [*Prockop and Chichkova*, 2007] causing a number of symptoms. When CO binds to haemoglobin, it creates Carboxyhaemoglobin (COHb). Typical health effects associated with low levels of COHb include minor headaches, dizziness, nausea and dyspnea (difficulty in breathing). As the concentration of COHb to Hb rises, neurological effects such as confusion, loss of short-term memory and visual disturbances occur. Finally, very high concentrations can cause seizures, coma, cardiopulmonary dysfunction and death. Many studies have found that there may also be delayed neuropsychiatric impairment that manifests itself within two to twenty eight days after poisoning [*Raub*

et al., 2000; *Stewart*, 1975; *Varon et al.*, 1999].

Mid to low concentrations which are sustained over a long time, can have similar effects to higher levels in short time periods, so there may be a great deal of undocumented cases of CO poisoning in towns and villages surrounding long term peat burns. The unavailability or prohibitive cost of treatment means the negative health effects may go undiagnosed or untreated indefinitely [*Varon et al.*, 1999].

Particulate Matter

Incomplete combustion is also a source of PM. PM can be divided into several categories based on its aerodynamic diameter, with the two most commonly studied classes, <2.5µm ($PM_{2.5}$) and <10µm (PM_{10} inclusive of $PM_{2.5}$). Both chemical makeup and size dictate the health effects PM may cause. PM_{10} (also known as thoracic) can penetrate the lower respiratory system, while $PM_{2.5}$ or respirable particles penetrate into the gas-exchange region of the lung.

Many studies have been conducted into the health effects of PM_{10} and $PM_{2.5}$, many of which found a correlation between high levels of PM and an increase in premature mortality. Research has been unable to determine a safe level of ambient $PM_{2.5}$ or PM_{10} at which no ill health effects can be attributed [*Ostro and Chestnut*, 1998; *Rückerl et al.*, 2011]. Studies in Europe, by the *Air Pollution and Health: a European Approach* and in the USA, by the *National Mortality, Morbidity and Air Pollution Studie*s have found correlations between mortality rates and increases of PM_{10} concentration to be as high as 0.6% per $10ug.m^{-3}$ [*Le Tertre et al.*, 2002; *Samet et al.*, 2000].

Peatland fires are a large source of aerosols in Southeast Asia, either directly emitted as PM, or through the generation of secondary aerosols. These aerosol emissions have significant impacts on local and regional air quality and affect agricultural productivity through the reduction in solar irradiance reaching agricultural regions all across Southeast Asia, potentially reducing yields by up to thirty percent annually [*Chameides et al.*, 1999].

As such, accurate knowledge of emissions contributing to PM levels is an integral part of building reliable models of air quality.

1.3 Peat burning in Southeast Asia

Southeast Asian tropical peatland fires account for approximately 10% of the estimated total greenhouse gas emissions generated annually from deforestation and forest degradation [*Ballhorn et al.*, 2009; *Van der Werf et al.*, 2009]. An immense amount of particulates and gaseous carbon are emitted during the long smouldering burn times [*Page et al.*, 2002; *Turetsky et al.*, 2015]. Regular seasonal peatland fires not only degrade air quality but also destroy unique ecosystems, impact human health and regional economies [*Gaveau et al.*, 2014]. The smouldering nature of these burns promotes increased emissions of fine particulates, methane and other trace compounds, and these are generally trapped in the boundary layer [*Rein*, 2013]. An example of this occurred in 2015, where smoke from peatland fires in Indonesia blanketed most of Asian throughout September and October in a persistent plume of pollution [*Field et al.*, 2016; *Huijnen et al.*, 2016], which resulted in an estimated one-hundred-thousand premature mortalities [*Koplitz et al.*, 2016]. Given the long-range transport that these emissions can undergo, tropical peatland fires often affect larger areas of the globe [*Andreae*, 1983; *Edwards et al.*, 2006; *Viatte et al.*, 2015].

Previous Research

Previous research into determining emissions levels from tropical peat fires is very limited. Published studies are limited to measurement of the gaseous emissions due to degradation of tropical peatlands by microbial oxidation [*Hooijer et al.*, 2010], and laboratory burns attempting to understand gaseous emissions from peat burning [*Christian et al.*, 2003; *Stockwell et al.*, 2014; *Wilson et al.*, 2015]. These laboratory burns have reported emission factors for trace gases from boreal [*Stockwell et al.*, 2014], and temperate [*Stockwell et al.*, 2014; *Wilson et al.*, 2015; *Yokelson et al.*, 1997] peat using samples from Sumatra [*Christian et al.*, 2003] and Kalimantan [*Stockwell et al.*, 2014], Indonesia. Another laboratory study incinerated small amounts of peat to determine the emissions of methane and the fraction of elemental to organic carbon released as a function of temperature [*Kuwata et al.*, 2017]. *Kuwata* also showed the effect of previously burnt peat reigniting, in this case reducing methane emissions by an order of magnitude [*Kuwata et al.*, 2017]. The first field measurements of tropical peat emissions were conducted in Kalimantan in 2009, and focused on greenhouse gases [*Hamada et al.*, 2013]. Across these studies a great degree of variability is observed, some of which has been explained by bulk density of the peat soil [*Wijedasa*, 2016], or the previous burn history of the peatland [*Konecny et al.*, 2016].

Geron and Hays, [*Geron and Hays*, 2013] measured $PM_{2.5}$ emission factors from organic soil layers and peat fuels in North Carolina and found significant variability in EFs between sites, ranging from $9 g.kg^{-1}$ to $79 g.kg^{-1}$. Despite the large impact caused by topical peat fire emissions, until recently there have been no emission factors for $PM_{2.5}$ in literature, with previous premature mortality estimates being extrapolated from measurements of other fuel types [*Giglio et al.*, 2013; *Lelieveld et al.*, 2015; *Van der Werf et al.*, 2010].

The first comprehensive field measurements of gaseous and particulate emission factors from burning tropical peat were conducted by Stockwell and co-workers [*Stockwell et al.*, 2016]. They report emission factors for trace gases and aerosols from Indonesian peat fires including $PM_{2.5}$, from seven different sampled smoke plumes at two separate peat fires. The $PM_{2.5}$ emission factors reported ranged from 15.7 to 29.6g/kg of dry peat consumed. These emission factors reported are presently the only emission factors for $PM_{2.5}$ from tropical peat fires in literature. The cause of the high variability they found has not previously been identified. Despite the overwhelming evidence for the large number of premature mortalities attributed to a rise in $PM_{2.5}$ pollution [*Beelen et al.*, 2014; *Lelieveld et al.*, 2015], and the high number of peat fires in Southeast Asia [*Hu et al.*, 2018], the emissions from these fires remains poorly understood. The work presented in this Master's thesis aims to contribute to a better understanding of the emissions of $PM_{2.5}$ emissions from tropical peat fires, so that the impact on air quality in the region can be modelled better in future.

1.4 Aims of this thesis

The Original aims of this thesis

1. To test and validate the instruments to be used in this project within a controlled smoke chamber at the Victoria University Werribee site (As explained in Chapter 2);

2. To determine particulate ($PM_{2.5}$) emission factors from tropical peat fires in peninsula Malaysia, through in-situ measurements. These will be conducted using the following instruments (also validated at the Werribee smoke chamber): an *Ecotech Aurora 1000g Integrating Nephelometer*, a *Thermo-Scientific Model 48i Gas Filter Correlation Carbon Monoxide Analyser*, a *TSI DustTrak DRX-8533 Desktop Model Aerosol Monitor*, and four *MSA Altair Pro Single Gas Detectors* (As described in Chapters 2 and 3);

3. Due to the possibility of limited field work in South East Asia, additional personal exposure measurements were planned locally. This campaign aimed to obtain measurements of fire fighter exposure to carbon monoxide at hazard reduction burns conducted by the New South Wales Rural Fire Service. These measurements will be made using CO sensors which were validated at the Werribee smoke chamber and will contribute to a study estimating total exposure to a range of toxins (As detailed in Chapter 2);

Additional aims

Due to the success of the initial Malaysian campaign, focus of this work was changed to put more effort into understanding the interesting results from the Malaysian peat fires and leaving less time to develop the fire fighter exposures work. This generated an additional aim.

To undertake laboratory burn studies to verify theories developed from analysis of initial fieldwork about the effect of the ash layer on particulate emissions (As shown in Chapter 4);

Chapter 2: Methods

The most suitable instrumentation to use for measurements of emissions from fires depends on the species of interest. Whereas open path methods average a concentration along a path, in-situ instrumentation sample from a single point in space. For the latter, care is required when comparing in-situ instruments so there are no biases introduced from improperly mixed gases. The primary aim for this campaign is to determine an emission factor of $PM_{2.5}$ for tropical peat fires, and a variety of in-situ instrumentation were chosen and deployed to help with this endeavour. These include; a Thermo Scientific *Model 48i Gas Filter Correlation CO Analyser*, a TSI *DustTrak-DRX Aerosol Monitor 8533*, an EcoTech *Aurora 1000 Integrating Nephelometer*, four *MSA Altair Pro* CO *Single Gas Detector* and two EcoTech *MicroVol-1100 Low Flow-rate* Air Sampler. A description of each of these instruments and an explanation of how they work is given below in section 2.1. The calibration and testing of these instruments in a dedicated smoke chamber is described in section 2.2. Finally, in this chapter, the deployment of personal monitors to measure the exposure of fire-fighters to pollutants emitted from hazard reduction burns is described briefly in section 2.3.

2.1 Instrument Descriptions

Thermo Scientific Model 48i Gas Filter Correlation CO Analyser

The Office of Environment and Heritage (OEH), Lidcombe office, provided a Thermo Scientific *Model 48i Gas Filter Correlation CO Analyser* on loan with a full service history. OEH have also provided a calibration service using an Environics 6100 (S/N: 6114) gas dilutor which had been calibrated on the 18th of July 2016 and a gravimetric standard cylinder of 5092 ± 41ppm CO. Calibration of the Model 48i was conducted at the following concentrations of CO; 0.0ppm, 4.9ppm, 9.9ppm, 19.8ppm, 24.7ppm, 29.7ppm and 39.6ppm. This calibration was conducted prior to all fieldwork campaigns and after returning from both Malaysian campaigns on the 26th September 2016, 22 February 2017 by the Office of Environment and Heritage, Lidcombe, NSW.

The *Model 48i CO analyser* operates on the principle that CO absorbs IR radiation at a wavelength of 4.6 microns. The analyser contains an infrared source with a path that passes through the sample cell and alternately also passes through a CO cell or a N_2 cell, as seen in Figure 1. The CO cell fully attenuates the infrared beam across the CO absorption features, to prevent any additional absorption within the sampling cell, thus giving a reference beam. The N_2 cell is transparent to the infrared radiation produced and thus any attenuation is due solely to CO in the sample gas. The analyser uses an internally stored calibration curve to linearize the non-linear nature of infrared absorption over any range up to a concentration of 10,000ppm CO [*Thermo Fisher Scientific*, 2007].

When sampling in the field, flexible inlet tubing with a PM filter was used to provide sampling from the same location as the PM measurement inlet. The exact experimental set-up is described in detail in Chapter 3 and Chapter 4.

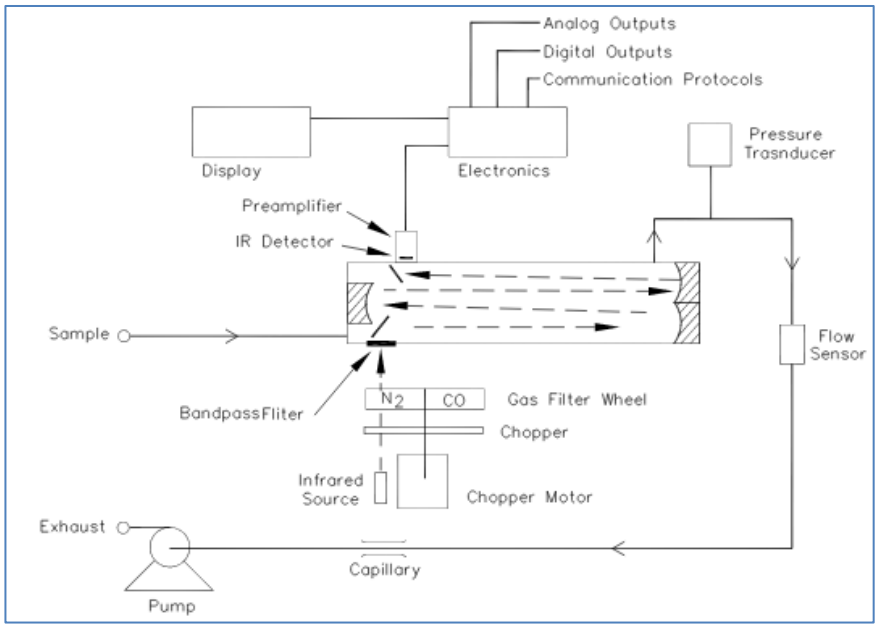

Figure 1 Model 48i Flow Schematic: used with permission of Thermo Fisher Scientific [*Thermo Fisher Scientific*, 2007].

Aurora 1000 Ecotech Nephelometer

The OEH, Lidcombe office provided an Ecotech *Aurora 1000 Integrating Nephelometer* for use in this Masters project. The Aurora 1000 measures the scattering coefficient of light due to particulate pollution (σ_{sp}), reported as inverse megametres (Mm^{-1}). It is the measurement of visibility, the higher the concentration of PM, the greater the scattering (σ_{sp}) and the lower the visibility. The Nephelometer used employed a narrow band 512nm (green) light source.

Light attenuation occurs by scattering off objects or absorption, in the atmosphere this is primarily by gas molecules and PM. σ_{ext} is the extinction coefficient, determined from the addition of σ_{scat} (scattering coefficient) and σ_{abs} (absorption coefficient). Each of these can be broken down into the effect of gases and particulates. NO_2 and molecular carbon are the most significant absorbers of light, although unless they are in extremely high concentrations these effects are insignificant compared to the effect of scattering.

Hence, σ_{ext} is approximated to:

$$\sigma_{ext} \approx \sigma_{scat} = \sigma_{sg} + \sigma_{sp}$$

Equation 8 Relationship between Extinction coefficient and scattering coefficient

Where:

σ_{ext}	= extinction coefficient
σ_{scat}	= the sum of attenuation of light scattering
σ_{sg}	= scattering due to gas molecules
σ_{sp}	= scattering due to PM

Using the above assumption, the attenuation of light is expressed using the Beer-Lambert law:

$$I = I_0 \, e^{-\sigma_{ext} x}$$

Equation 9 Beer-Lambert law

Where:

I_0	= initial light intensity,
I	= intensity after distance x,
x	= distance,
σ_{ext}	= the attenuation of light, or extinction coefficient, sometimes symbol b used.

Visual range (*Lv*) is calculated from the extinction coefficient using Koschmieder's Formula:

$$Lv = 3.912/\sigma_{ext}$$

Equation 10 Koschmieder's Formula

During operation, the instrument undergoes three measurement steps to determine the extinction coefficient. These stages are the shutter count, dark count and measurement count. The shutter count (C_{sh}) happens every thirty seconds for four seconds, where a glass shutter of known transmittance closes over the path length, providing a gas free

path between the light source and photomultiplier tube. This allows for automatic adjustments accounting for variations of intensity in the system, such as changes in bulb intensity. The dark count measures background light and imperfections in the photo multiplier tube and detector by shutting off the light source and measuring background light in the sample vessel. Finally, the measurement count (C_m) samples with the shutter (translucent glass) open and the light source on, allowing measurement of the scattered light.

The use of these three steps determines a measurement ratio. This measurement ratio is directly proportional to σ_{scat} as C_{sh} is through the known transmittance. This provides the ability to maintain reliable measurements despite changes in temperature and light intensity. Changes to the system will maintain the measurement ratio; however, changes to σ_{scat} caused by sample changes will only vary the C_m value. [*Ecotech*, 2009]

$$MR = C_m/C_{sh}$$

Equation 11 Measurement Ratio

The assumption that scattering from gaseous particles, or Rayleigh scattering is subtracted during the zeroing step of calibration and that the effect of absorption of light by particles is minimal except when concentrations of NO_2 and soot are high, allows the Aurora to provide an accurate representation of light scatter, or visibility with regard to PM [*Ecotech*, 2009]. The NSW OEH states that unsafe levels of scattering due to light scattering particles start at $2.1x10^{-4}m^{-1}$ or $2.1x10^{-10}Mm^{-1}$ averaged over 1 hour [*NSW OEH*, 2014].

Calibration of the Nephelometer was provided by the OEH at the same intervals as the Model 48i, using a calibration standard of pure FM200 (1,1,1,2,3,3,3-Heptafluoropropane). Calibration occurs by using filtered particulate free air and a calibration gas of known σ_{scat}. The zero calculation uses zero air to subtract the Rayleigh scattering from σ_{scat} and the span uses certified FM200.

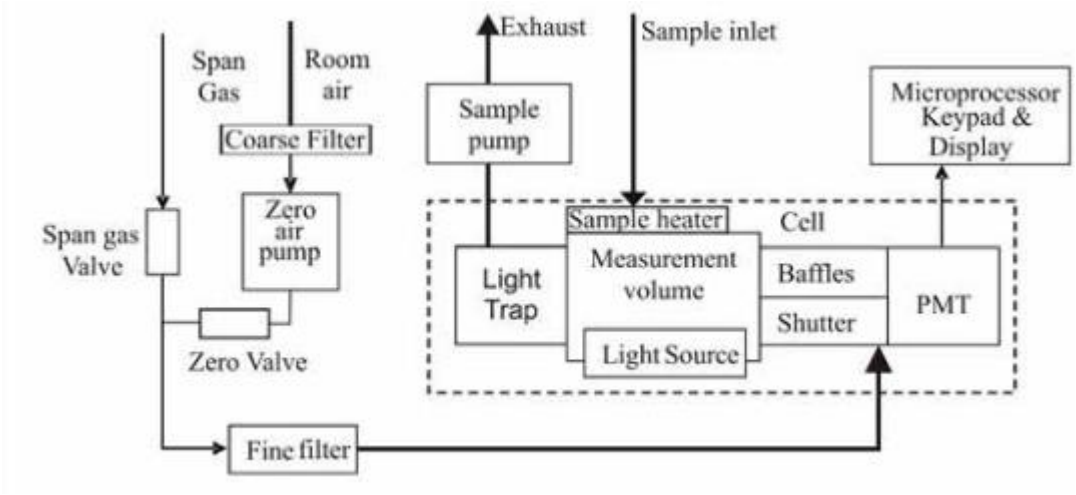

Figure 2 Ecotech Aurora 1000 block diagram of internals: used with permission of Ecotech [*Ecotech*, 2009].

TSI DustTrak-DRX Aerosol Monitor 8533 Desktop Model

A TSI *DustTrak DRX 8533 Desktop model Aerosol Monitor* (on loan from the OEH, Lidcombe office), conducted real-time accurate particle monitoring. The DustTrak uses a proprietary light scattering method to determine both size and concentration of PM allowing PM_1, $PM_{2.5}$, Respirable/PM_4, PM_{10}/Thoracic and total PM, to be measured simultaneously. The pump draws sample air through an omnidirectional inlet with a rain cap mounted to the top of the environmental housing. As shown in Figure 3, the sample is diluted using a sheath of filtered sample air to prevent clumping of PM and prevent PM landing on any optics in the instrument. A laser diode emits light that is diffracted through a collimating lens and a cylindrical lens to create a thin sheet of light. Sample is passed through this sheet and scattered light is reflected and concentrated by the gold-coated mirror onto the photo-detector. Using pulses of light and proprietary algorithms, the concentration of each bracket of PM sizes is determined and stored internally at user-defined intervals for later retrieval [*TSI Incorporated*, 2012]. Due to the methods employed by the DustTrak and the difference in surface properties of different particles, a correction factor determined by comparison to gravimetric results of a similar fuel source should be used.

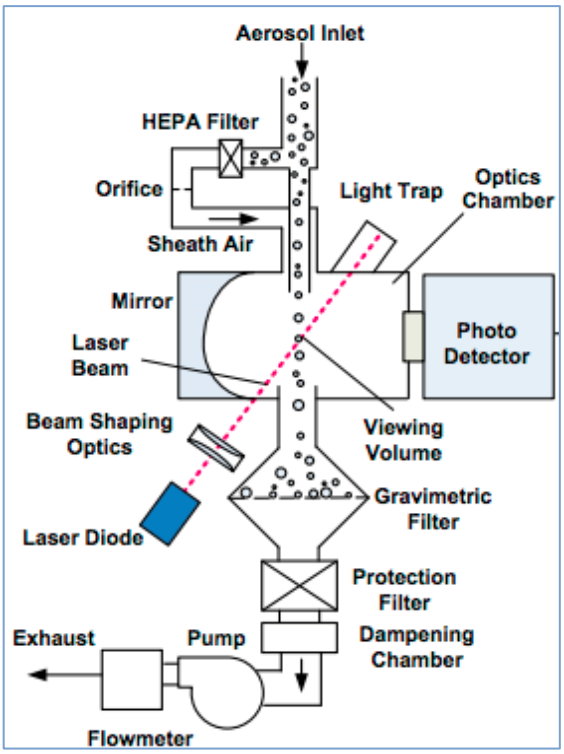

Figure 3 TSI DustTrak DRX Aerosol Measurement Diagram: Diagram courtesy of TSI Incorporated [*TSI Incorporated*, 2012].

A recent study discovered an issue with baseline spikes when DustTrak monitors are run for extended periods without running a zero calibration. This issue has minimal effect when measuring high concentrations of PM and with regular zero calibrations [*Rivas et al.*, 2017].

MSA Altair Pro Single Gas Detector – Electrochemical

The *MSA Altair Pro Single Gas Detectors* used in this study employ a single gas sensitive electrochemical sensor. The main gas monitor used for personal exposure measurements was carbon monoxide. A deployment of additional monitors for HCN, NH_3 and SO_2 was tested at some burns but due to calibration issues and suspected interferences, the results were deemed unreliable. The MSA personal exposure monitors used in this Masters research are designed to be a simple to use, single button, gas measuring and logging instrument. Prior to each deployment of these instruments a fresh air background is conducted, and the instrument is set to zero using background concentrations of the gas of choice. In the case of CO this is approximately 60-100 ppb, (much lower than the minimum detection limit of 1ppm to which this instrument reports). Second, a known concentration of CO (60±6ppm) is piped into the instrument at a rate of 0.25L/min, to achieve a span calibration [*MSA Safety Appliances Company*, 2011].

Figure 5 MSA Altair Pro Single Gas Detectors deployed to hazard reduction fires.

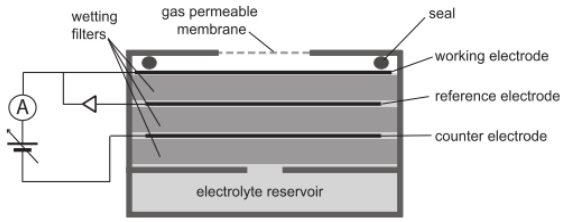

Figure 4 General schematic of an electrochemical cell. The gas permeable membrane and seal is used to prevent water and dust entering the cell. Throughout operation the working and counter electrodes maintain a fixed voltage bias: Reproduced with permission of Iq Mead [*Mead et al.*. 2013].

Electrochemical sensors within the MSA exposure monitors are low power, low-cost amperometric sensors, which are designed to respond to gases at concentrations at the parts-per-million level. The sensors contain electrodes separated by hydrophilic separators (also known as wetting fillers), which allow ions to flow between the electrodes via capillary action. The working electrode generally promotes oxidation of species of interest. A catalyst is normally coated to create a large surface area that is optimised to promote reaction with the species of choice. Electronic charge is generated by this redox reaction, which in turn creates a different charge potential at the working electrode than the reference electrode. This reaction is geared to be much faster than the speed of gas diffusion across the membrane, hence detected charge is proportional to concentration of the reacting species [*Stetter*, 2008]. In the presence of a measured gas the counter electrode changes potential to compensate for the charge generated by the working electrode. The potential of the working electrode is maintained using the reference electrode, providing a difference between the working

and counter electrodes. This difference in potential is measured by additional electronics in the systems to determine concentration of the selected gas-species [*Mead et al.*, 2013].

2.2 Werribee Smoke Chamber – Calibration of Instruments

Between the 24th and the 28th of May 2016, the Victorian Environmental Protection Agency conducted a series of controlled smoke chamber burns at the Victoria University, Werribee campus, Victoria, Australia. The primary purpose for this exercise was the comparison and evaluation of various PM-measuring instruments, with a focus on $PM_{2.5}$. The chamber's regular purpose is to create and analyse flashover and backdraft scenarios. A flashover occurs when pyrolysis of various fuel sources occurs to a point where flammable gases ignite in a near-simultaneous fashion, consuming the room in flame. A backdraft is a similar scenario that occurs when oxygen is rapidly introduced to the gases fuel mixture creating an explosive reaction (often as a result of having a door opened). The hood seen below is designed to catch such events by evacuating flammable gases and flame to the atmosphere via a series of vents and an industrial scale extraction fan.

Figure 6 Top-Left-Smoke test chamber, exhaust fan can be seen centre top and the exhaust piping can be seen leaving the right hand side of the image; Top-Right-The exhaust vent; Bottom-Center- The layout of instrumentation, Victoria University, Werribee, Victoria.

For the purposes of the PM chamber test, a modification to the door allowed a controlled flow of smoke to enter the room, with excess smoke evacuated by an industrial scale fan (see Figure 6). To ensure adequate mixing of the smoke, two fans were mounted centrally within the chamber to mix the smoke and additional sampling inlets were installed to test the mixing in real-time, using the Victorian EPA's DustTrak, as per Figure 7 and as described in Table 1.

Table 1 A summary of the real-time measurements of smoke concentration through the chamber at different locations, testing for homogeneity. NB the concentration values here are uncorrected by the Partisol (gravimetric) results.

Tube #	Position	Height (cm)	Time on	Time off	Visual reading (mg/m^3)
1	Bottom right	23	10:25	10:30	1.17
2	Back middle	63	10:30	10:35	1.17
3	Back middle	137	10:35	10:40	1.06
4	Left side	170	10:40	10:45	1.11
5	Left side	60	10:45	10:50	1.12
6	Left middle	160	10:50	10:55	1.07
7	Left middle	75	19:55	11:00	1.10

Table 1 describes the position of the additional sampling inlets used by the Victorian EPA's DustTrak to test for homogeneity. The position is relative to the entrance of the chamber, where smoke was introduced to the chamber. Height denotes distance from the floor of the chamber, as many instruments were sampling from different heights. Time on and off were used to assign measurements to the associated test location, and visual reading was an estimate of average PM readings over the five-minute test window.

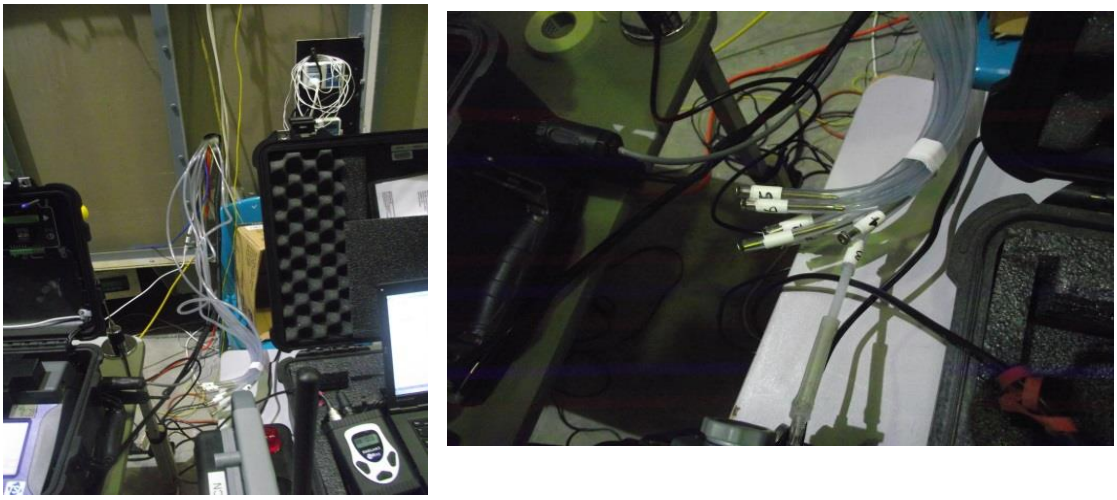

Figure 7 Left- Inlets for DustTrak testing of homogeneity; Right - Inlets reaching DustTrak.

Figure 8 shows the fuel sources used throughout this experiment. Both the wood smoke and coal smoke experiments were conducted by igniting the selected fuel source with a coke igniter, and prolonged burning was facilitated by use of a gas stove. The diesel test used a 2016 Mitsubishi Triton Ute running on diesel fuel. The exhaust was piped through flexible tubing into the chamber. The Ute engine ran at idle speeds throughout the test to maintain the diesel exhaust levels. As shown in Figure 9, the smoke from burning samples was fed into the chamber by a purpose built manifold, which allowed excess smoke to be evacuated from the area (see the Top-Right image of Figure 9). Despite this manifold smoke levels were still too high. To combat this, the manifold and burning samples were moved away from the entrance by 500mm, thus reducing the amount of direct smoke added to the chamber.

Figure 8 Top-Left- Sticks and leaves used for wood smoke test; Top-Right - ground coal dust burnt for coal test; Bottom- Exhaust fumes used for diesel test.

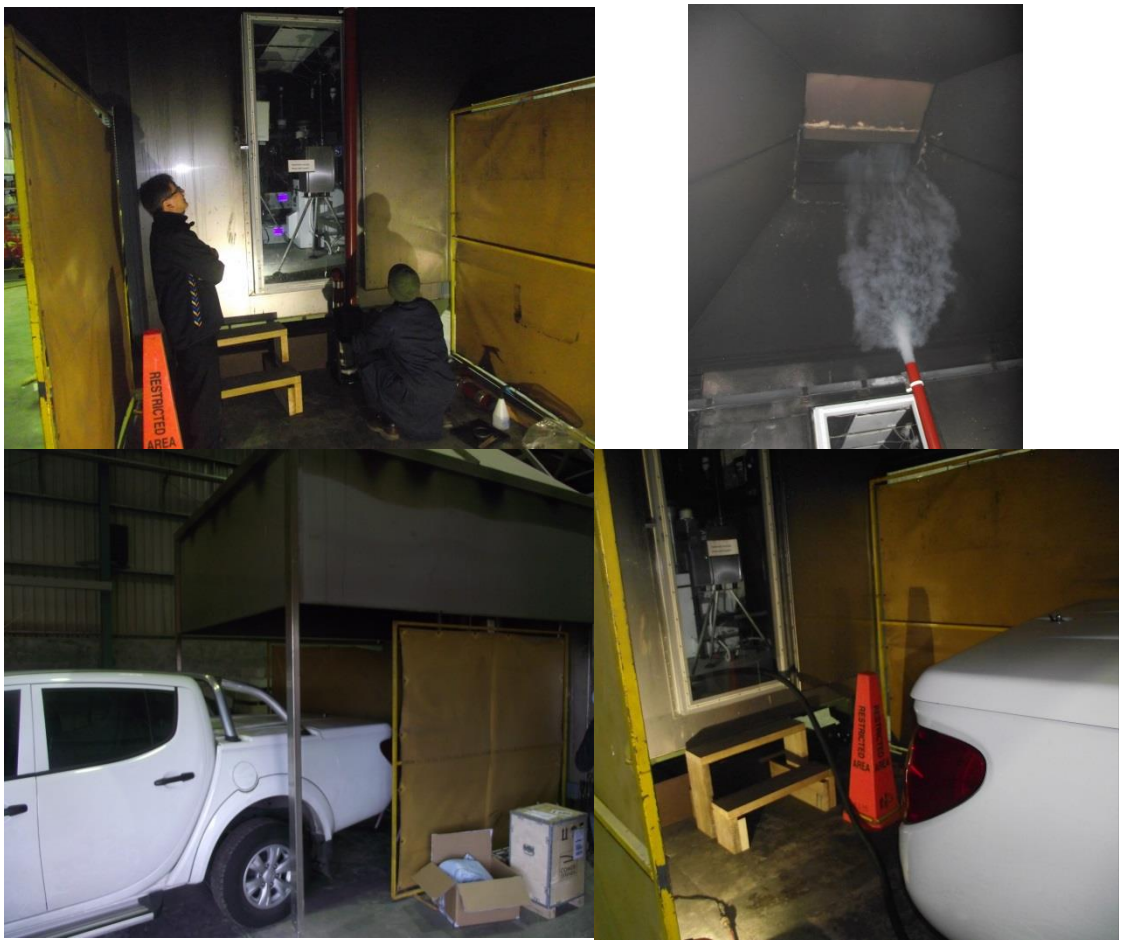

Figure 9 Top-Left - Addition of smoke to the test chamber; Top-Right - excess smoke being evacuated; Bottom-Left - setup for diesel test; Bottom-Right - Diesel exhaust being piped into chamber.

Additional instrumentation used in this test included;

- Wollongong University (Run by Christopher Roulston)
  - *DustTrak-DRX 8533 Desktop Aerosol Monitor*
  - *AQMesh* – Instrument designed to have various gas measuring modules installed, all data is transferred to the remote AQMesh server.
  - *Airbeam* (1) – Community science particulate measuring project, measures PM by employing a small and cheap to produce LIDAR. Also tracks GPS location to allow communities to map their city health.
  - *Airbeam* (2)
  - *Aurora 1000 Integrating Nephelometer*
  - *Thermo Scientific Model 48i CO Gas Filter Analyser*
  - *4x MSA Altair pro CO Single Gas Detector*
  - *MSA Altair pro NH_3 Single Gas Detector*
  - *MSA Altair pro SO_2 Single Gas Detector*
  - *MSA Altair pro HCN Single Gas Detector*

- Golder Associates (on behalf of Victorian EPA)
    - *Partisol 2025 sequential air sampler* – Gravimetric analysis, pumps a known volume of air through pre-weighed filters. After test filters were conditioned and weighed.
- LSA
    - *BAM5014i* (1) – Thermo Fisher - Beta Continuous Ambient Particulate Monitor. Real-time continuous measurement of the mass concentration of suspended and refined particulates by measuring the attenuation of beta radiation across a known area of fibrous filter tape upon which particles are deposited.
    - *BAM 5014i* (2) (Run on behalf of EPA)
    - *ADR* (1) – Area Dust Monitor – Real-time measurement and categorisation of PM, PM_{10} to PM_1 through a sensitive light-scattering photometer (nephelomter).
    - ADR (2) (Run on behalf of EPA)
- Ecotech
    - *BAM 1022* – Met One Beta Attenuation Method instrument. Similar to BAM1022
    - Met One unit – New in development BAM1022 unit.
- Envisys
    - *Aeroqual AQM65* – Real-time air monitoring station. Uses a nephelometer to measure particulates, Profiler particle counter.
- Victoria University
    - *Nova PM sensor – SDS 011 Sensor* – A real-time low size, low cost sensor, used to validate lower end instrumentation against industry standards like the BAM1020.
- TES
    - *Dustmaster* – Real-time laser particulate monitor. Simultaneous measurements of; total PM, PM_{10}, PM_4, $PM_{2.5}$ and PM_1.
- Dius
    - *Dylos* – Another low cost particulate monitor using light scattering.
- Attentis
    - *Flamesniffer* (1) – In development instrument that measures various gases and PM.
    - *Flamesniffer* (2)
- Ecodev
    - *Vesda*
- Victorian EPA
    - *SmokeTrack*
    - *Citizen Science unit*
    - *AreaRae CO*
    - *AreaRae NO_2/SO_2*
    - *AreaRae other*

Figure 10, shows the setup of instruments within the smoke chamber. Shelves were used to vertically line up instrument inlets. (Instruments are not to scale). Dark blue boxes denote instruments run at the test as part of this Master's project, and the bracketed values are the inlet height in millimeters. Model 48i CO monitor was shelved bellow all other instruments, but due to its flexible inlet, the sampled location was collocated with the nephelometer.

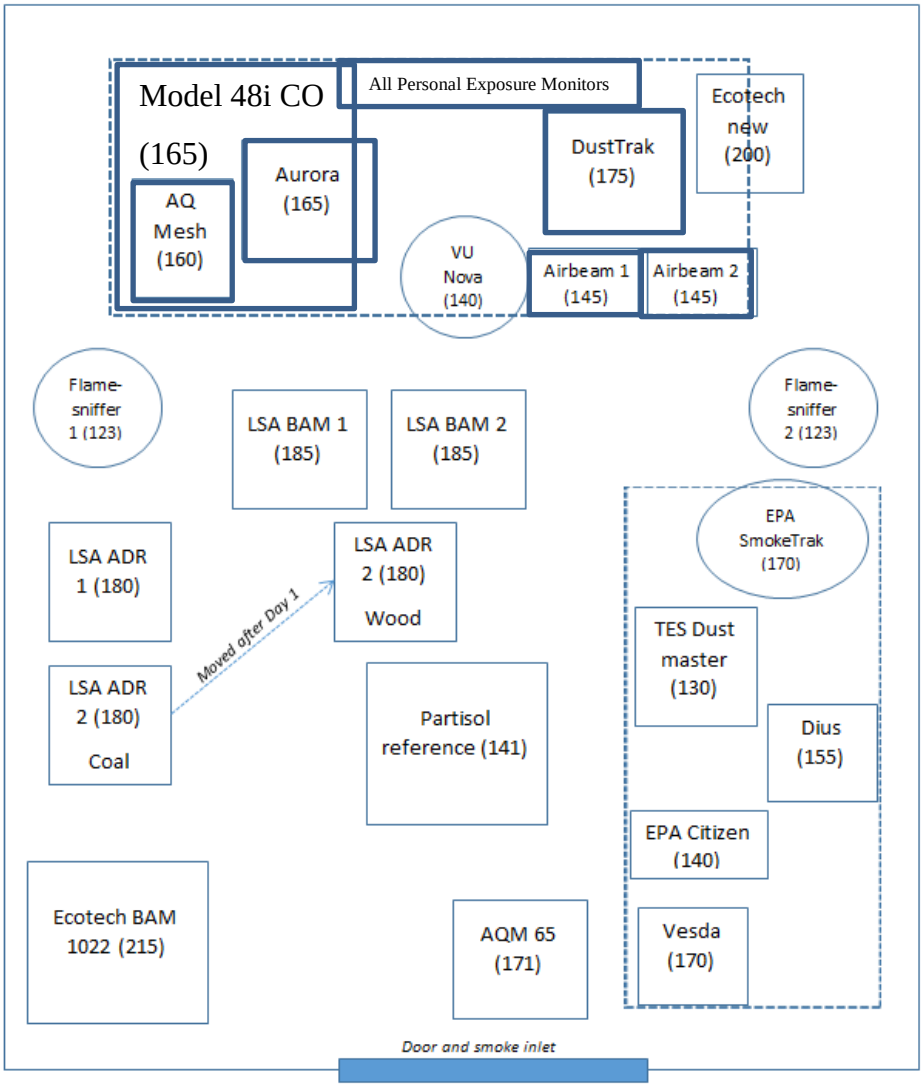

Figure 10 Instrument layout for Werribee smoke chamber test: adapted from Victorian EPA smoke chamber summary notes (not currently published).

The primary purposes for involvement in the Werribee smoke chamber experiment was the validation of instrument accuracy. This was achieved via comparison to other real-time instrumentation on the market and also to gravimetric standards to determine a correction factor for the DustTrak by calibrating it in wood and coal smoke. This calibration used the results from the *Thermo Fisher Scientific Partisol 2000i-D Dichotomous Air Sampler*, as gravimetric samples are considered the most accurate and reliable measurements of PM over long periods.

2.3 Results of Instrument Inter-comparisons

The results from this experiment were used to derive a correction factor for the DustTrak and for the validation of the *MSA Altair Pro CO Single Gas Detectors* against the *Thermo Scientific Model 48i* CO monitor.

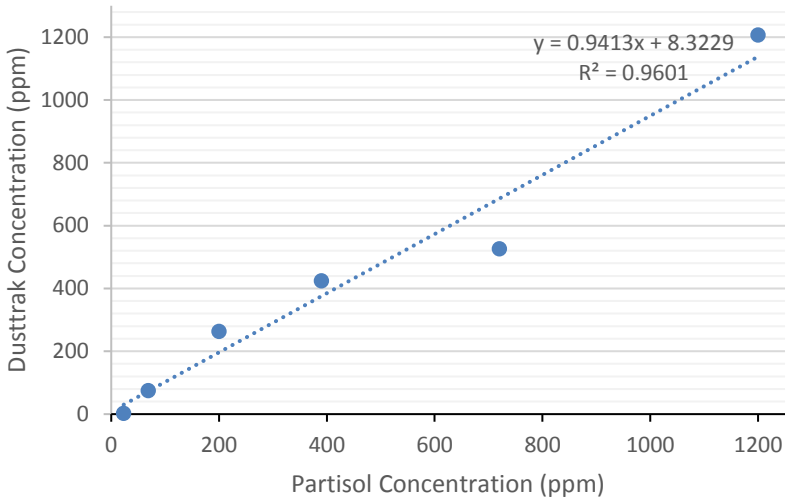

Figure 11 Correlation plot for DustTrak against gravimetric Partisol, Wood smoke.

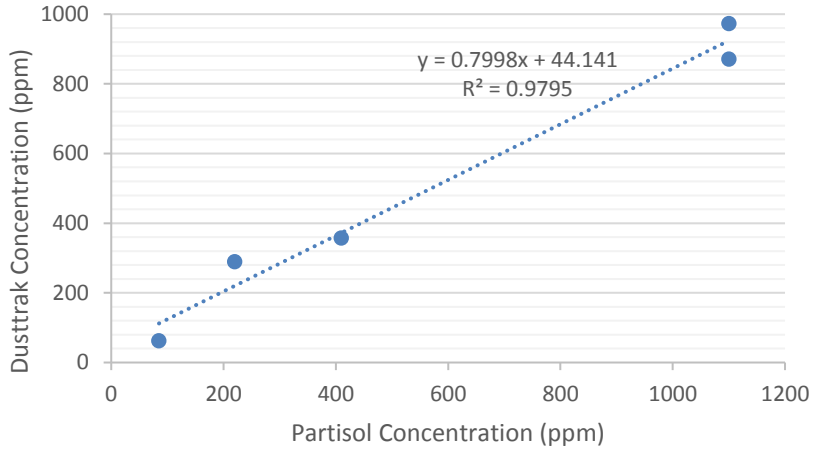

Figure 12 Correlation plot of DustTrak against gravimetric Partisol, Coal smoke.

Figure 11 and Figure 12 show the correlation between the DustTrak and the gravimetric Partisol measurements, for wood and coal smoke respectively. Each point represents the concentration determined gravimetrically from one Partisol filter (on the x-axis) and the average DustTrak concentration integrated over the same time (on the y-axis). As can be seen, there is a good correlation between the DustTrak and gravimetric results, providing an R^2 of 0.96 for wood smoke and an R^2 of 0.98 for coal. Of more use are the values of the gradients from these regression plots, because these provide the relative response of the instruments and hence the calibration of the DustTrak to the gravimetric standard from the Partisol instrument. When calculating

the DustTrak's correction factor this way, I saw that its response is about 6% low when compared to gravimetric measurements in wood smoke, and 20% low when compared in coal smoke. This difference is primarily caused by the difference in particle size distribution with coal smoke having a larger mean diameter than wood smoke [*Zhang et al.*, 2012].

When comparing the instruments' values in more detail, (due primarily to the low number of points on the regression plots), I found that the uncertainty in the calibration factor was quite high. Another method applied to the data to find a correction factor, was to take the ratio between DustTrak and Partisol reading at each point and average it. Analysing the wood-smoke data this way indicated a positive bias of approximately 7% in the DustTrak readings, with a large standard deviation. Finding these conflicting *biases* it was determined that the DustTrak agreed with the gravimetric analysis for wood-smoke within the uncertainties of the calibration. Tropical peat smoke is expected to be closest to wood-smoke in nature, but its particle size distribution could fall between that of wood and coal. Thus it was decided that the DustTrak values would be used uncorrected (as per the calibration in wood-smoke), but with a large uncertainty assumed. The largest bias from the smoke chamber tests (of 20%) was taken as the uncertainty in measurements taken by the DustTrak throughout the Malaysian campaigns. Another reason for using an uncertainty as high as ± 20%, is that the validation testing for the DustTrak only covers the range of measurements through which calibration occurred. As described in Chapter 4 and Chapter 5, values measured during the laboratory and field campaigns were much higher than those in the Werribee smoke chamber experiment.

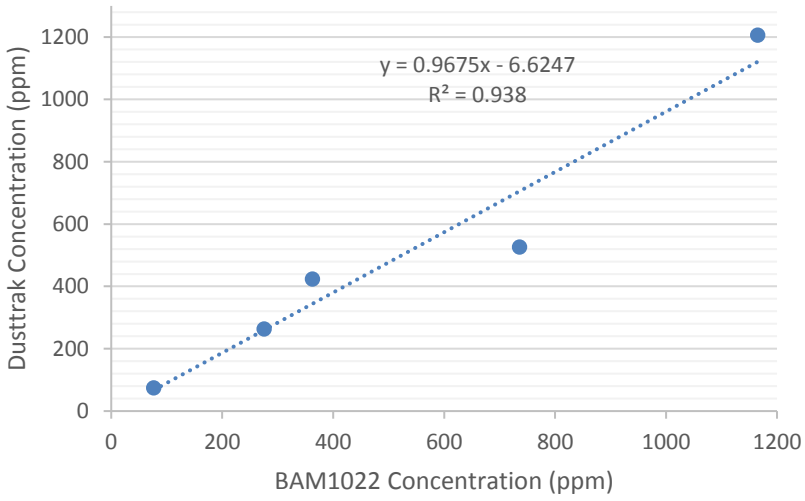

Figure 13 Correlation plot for DustTrak against real-time BAM1022, Wood smoke.

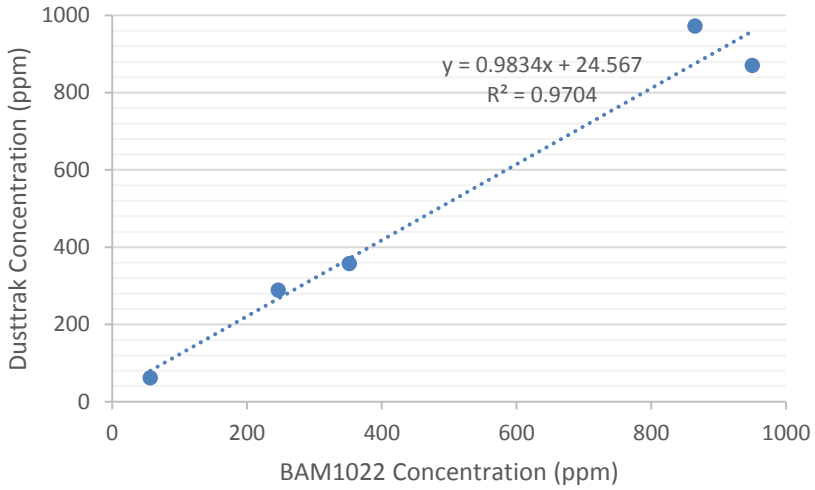

Figure 14 Correlation plot for DustTrak against real-time BAM1022, Coal smoke.

Figure 13 and Figure 14 show the correlation of the DustTrak against an industry standard, the BAM1022. Although both sensors use very different methods to measure PM, (the DustTrak uses light scattering and the BAM1022 uses beta radiation attenuation methods), there is a high level of agreement between the two for both wood and coal smoke sources. The DustTrak again shows a low negative bias across both fuel types, being approximately 3% low with an R^2 of 0.94 when compared to the BAM1022 for wood smoke and 2% lower with an R^2 of 0.97 for coal smoke. This shows that both the DustTrak and BAM1022 miss or underestimate some of the smaller particles that are captured by the gravimetric analysis. Their obvious benefit is in producing real-time observations at high temporal resolution (e.g. minute averaged data), that can capture events that occur over short time periods. These can be used in tandem with other continuous in-situ instrumentation, such as CO concentration measurements, as was the purpose of later work. The high level of agreement between the industry standard BAM1022 and the DustTrak provides a higher degree of confidence when deploying the DustTrak for additional fieldwork.

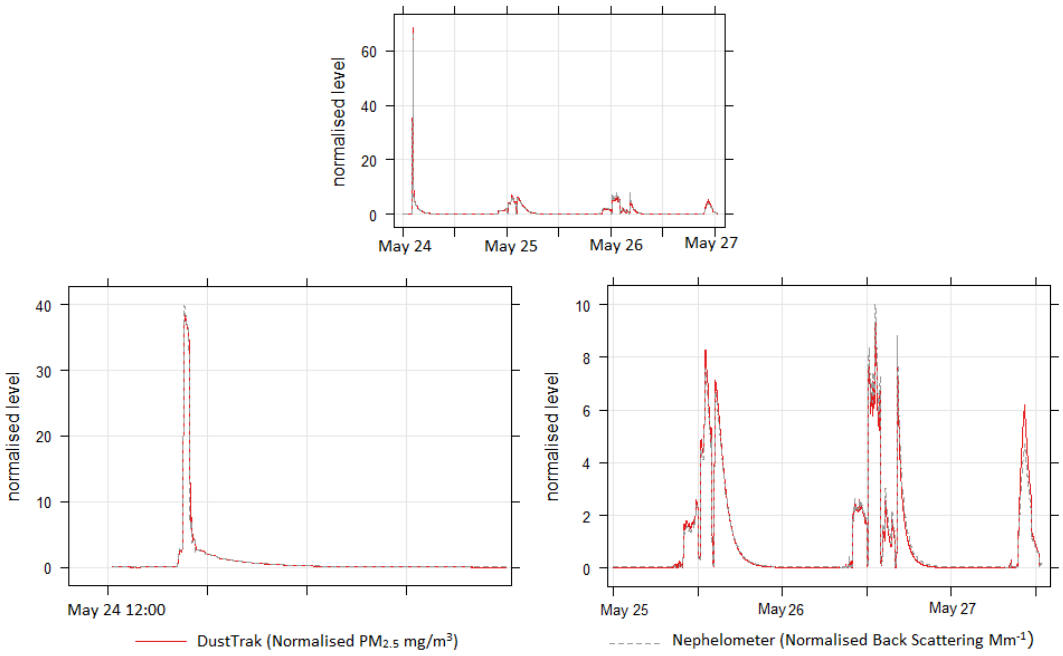

Figure 15 Top-Centre: Total timeseries of normalised DustTrak and Nephelometer data from the Werribe smoke chamber. Bottom-Left: An enlarged view for the fire peak shown in the complete serise above. Bottom-Right: An enlarged view of the remaining three peaks from the complete series above.

Figure 15 shows the normalised time-series of the DustTrak and Nephelometer, illustrating the high level of agreement between the two instruments across a range of $PM_{2.5}$ concentrations. The normlisation of data removes unit differences and instead displays the total magnitude of relative measurements, crossing the gap between the $PM_{2.5}$ measured by the DustTrak and the Visibility measured by the Nephelometer. The above time series were all taken at the Werribee smoke chamber experiment. The enlarged peak on the Bottom-Left shows the wood smoke burn conducted on the 24/05/2016. The size of this peak is exceedingly large than the other two due to experimental error, causing an excess of smoke to be introduced into the smoke sampling chamber, and hence threw off the scale for the other three peaks. The final three peaks shown in the graph on the Bottom-Right shows the remaining three days of testing which included in order second wood smoke test, coal dust and finally the diesel exhaust fumes. As can be seen across all days, the overall normalised trend show both the DustTrak and Nephelometer trace very well regardless of fuel source, this relationship can then be used as a confirmation of instrumentation state in future field studies.

The three graphs indicated in Figure 16 show the correlation between the DustTrak and nephelometer for each fuel type. The left shows the relationship for coal smoke as each mg/m^3 of PM detected by the DustTrak converts to 1672^{-1}Mm with a strong relationship shown by the R^2 of 0.99. The centre graph shows the effect on this relationship of the smaller diesel particles, with the nephelometer reading 1403 $^{-}$Mm per mg/m^3 measured by the DustTrak with an R^2 =1, showing that the smaller particles cause less light scattering and hence a lower response from the nephelometer. The right-hand graph shows the relationship when measuring

particulates created by wood smoke. The linear relationship once again has an R^2 of 1, and a gradient of 1968 $^{-}$Mm per mg/m^3 measured by the DustTrak. The colour scale shows the relative humidity of nephelometer readings, the lack of effect caused by this to the relationship between the DustTrak and nephelometer suggests the heater is functioning correctly and removing excess moisture from PM. There was a high degree of moisture in the diesel test. This may have been due in part to the local weather conditions at the time, but more likely due to the greater amount of moisture in the diesel exhaust. The strong linear relationships between these two instruments at the smoke chamber experiments, indicates that the nephelometer can be used as an additional validation for the DustTrak readings obtained on the field campaign.

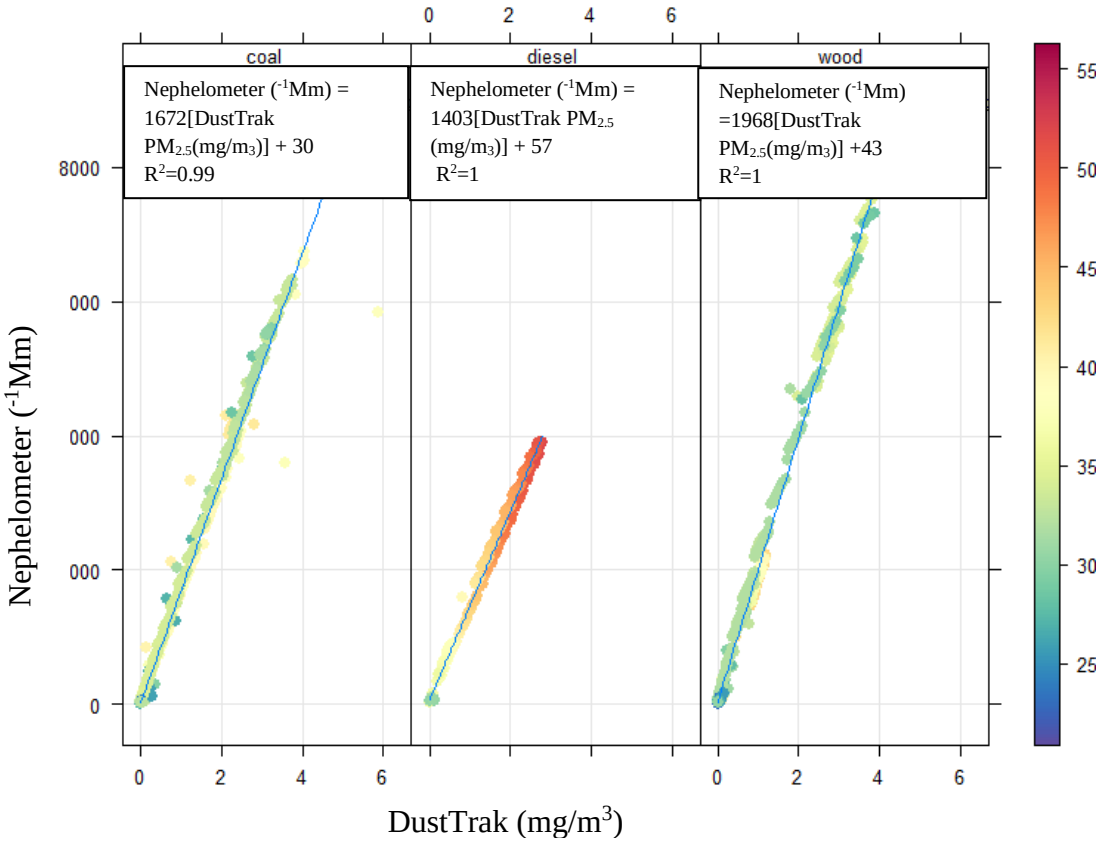

Figure 16 Correlation between DustTrak and Aurora 1000 nephelometer across three fuel sources. Left: Shows correlation with coal smoke. Middle: Shows diesel exhaust fumes. Right: Shows the correlation with wood smoke. The colour denoted on the right hand side shows the relative humidity as measured by the nephelometer.

Figure 17 shows a complete time series of the MSA Altair Pro CO monitors and the Thermo Scientific Model 48i CO monitor. As shown, (other than a few sporadic underestimations, primarily by sensor #2), there was a good level of agreement between the electrochemical sensors and the infrared absorption based Model 48i CO monitor. The values measured within this time series cover a large range of values that are expected to be experienced during the field studies. This provides confidence when using the personal monitors within smoke plumes generated by wood fires. The time series for the Model 48i is near continuous, while all personal monitors were removed for two hours each morning for data download and recalibration.

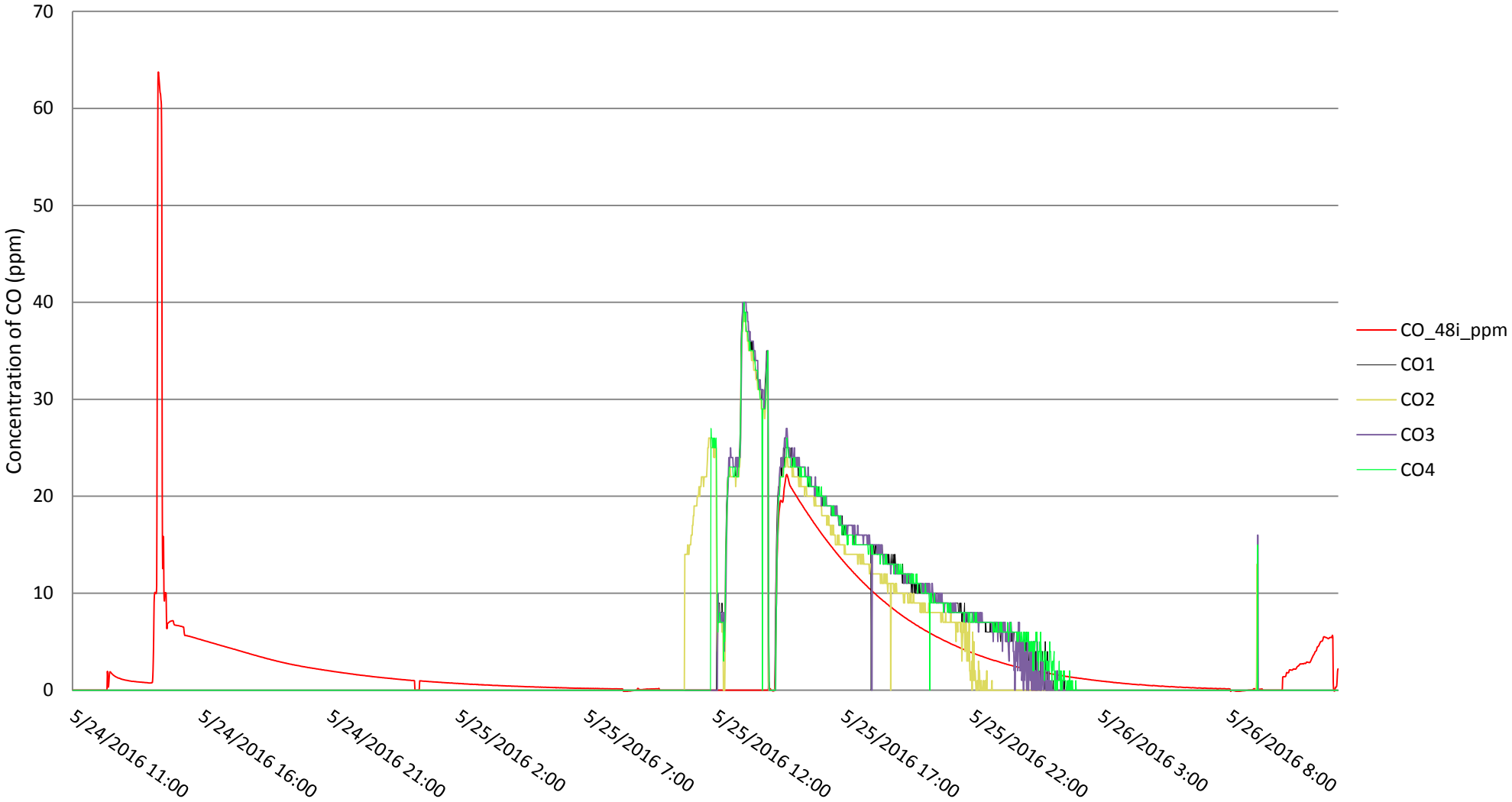

Figure 17 A time series showing the complete CO measurements, includes Model 48i CO readings and 4x MSA Altair Pro CO personal exposure monitors. It shows a close relationship between trends observed by the CO monitors and the CO analyser.

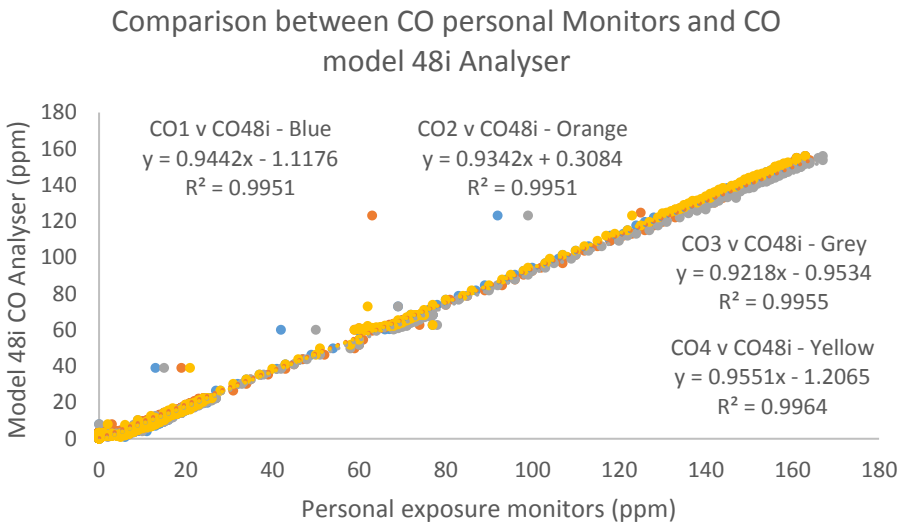

Figure 18 Correlation plot showing the correlation between the *Model 48i CO Analyser* and all 4 *MSA AltAir Pro personal exposure monitors*.

Figure 18 shows the correlation between all four personal exposure monitors and the Model 48i CO analyser. A strong correlation is observed across all four personal monitors when compared to the CO Analyser, showing R^2 values above 0.93 in all cases. There is a discrepancy at the lower end of concentration measurements, caused both by the detection limit of the personal monitors and their resolution of 1 ppm. This resolution also contributes to an overestimating of between 5% and 8% across the personal monitors when compared to the CO analyser. As previously mentioned, the high correlation across a wide range of concentrations shown between the *Model 48i CO Analyser* and the *MSA Altair Pro CO Monitors* provides confidence in the use of the exposure monitors for the planned fire-fighter exposure campaign during hazard reduction burns, as detailed in Chapter 2.3.

2.4 Summary of Findings from the Werribee Smoke Chamber Experiment

The results from this campaign showed high correlation and relatively low bias between the OEH provided *DustTrak-DRX 8533 Desktop Aerosol Monitor* and the gravimetric *Thermo Fisher Scientific Partisol 2000i-D Dichotomous Air Sampler* for wood smoke. The uncertainty in determining the bias, was as large as the correction factor itself and so the DustTrak will be used without a correction applied when deployed at the peat fires (since I expected the sensitivity of the DustTrak to peat smoke to be similar to that of wood smoke). The correlation between the DustTrak and the *BAM1022* also provided validation to using the DustTrak as a real-time monitor for PM emitted by wood and coal smoke sources.

The comparison of the *MSA Altair Pro CO Single Gas Detectors* to the *Thermo Fisher Model 48i Gas Filter Correlation CO Analyser* showed a negative bias in personal CO monitor #2, but all other monitors and the analyser showed both a high degree of correlation and accuracy. This provided evidence of the reliability of these personal monitors, while following the standard operating procedure of daily calibration.

The tests also provided evidence to support the accuracy and stability of the instruments after transport, and the long-term stability of the *Model 48i CO Analyser and Aurora 1000 Nephelometer*, as the instruments had been transported to Werribee and it had been approximately three months since their last calibration.

2.5 Personal Exposure Monitor Campaign

The initial field campaign for this Masters Research project focused on exposure data obtained from hazard reduction (HR) burns in New South Wales, Australia. The New South Wales fieldwork began with two studies conducted in early March 2016 at a 900ha hazard reduction burn in Mittagong (see Figure 19), and a second burn on Mt. Kiera.

The New South Wales fire-fighter exposure study used four personal CO monitors worn by individual firefighters. HCN and NH_3 monitors were also deployed (a single NH_3 monitor and a single HCN monitor ran in tandem with a CO monitor). They were attached to the chest as close to the breathing zone of each firefighter as possible, so as to allow the firefighters to maintain mobility and complete their duties, whilst still obtaining an accurate representation of the toxin being inhaled, as shown in Figure 20. The monitors recorded peak and average concentrations at one minute resolution.

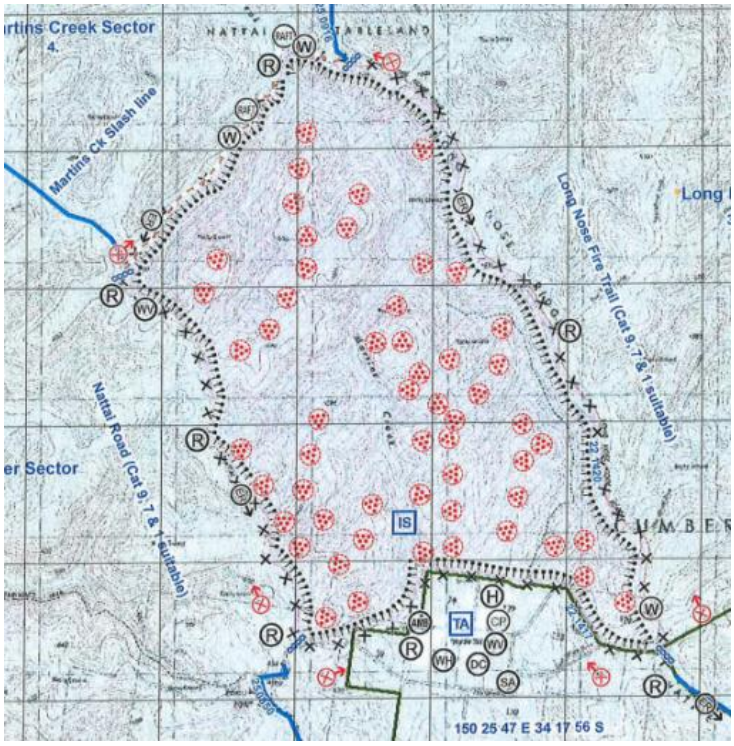

Figure 19 Map of the HR burn zone [*Pedroza et al.*, 2016].

Additional studies were planned during the hazard reduction burning season, (out of the wildfire season), in a similar fashion, but due to the combination of unpredictable weather and the success of the Malaysian campaign this work did not continue. Whilst similar to a previous campaign headed by Fabienne Reisen [*Reisen and Brown*, 2009], this study has its own merits, due to spatial variation of fuel types and temporal differences, coupled with the variety of monitors deployed.

The results from this work will provide a basis for estimating the magnitude of exposure to pollutants experienced by firefighters, and as a study such as this has not been completed in recent years, may provide insight into whether current fire ground training and behaviours have had an effect on toxin exposure levels. Although exposure may be influenced by an individual firefighter's behaviours, there has been a recent focus within the Rural Fire Service to reduce exposure to smoke. Spurred on by legislation and previous research, methods are employed to reduce smoke and pollution emissions from HR burns. Another important change in rules and

Figure 20 A volunteer fire-fighter with two MSA Altair Pro Single Gas Detectors attached to the chest area of his uniform.

regulations comes from the *Protection of the Environment Operations (Clean Air) Regulation 2010*, which dictates the general obligation to prevent or minimise air pollution [*NSW*, 2010]. This regulation is also give power by *Protection of the Environment Operations Act 1997*, which gives the EPA the power to prohibit burning of fires when its officers believe it will contribute to air pollution increasing to a high level or unwanted Air Quality Index (AQI). This overrides all other permits for the purpose of maintaining air quality [*NSW*, 1997].

The results of this study have been provided to Katrina Macsweeen from Macquarie University, Sydney, NSW. Due to the success of the Malaysian peat fire campaigns, I have ceased additional work into this study. Results are to be published in a journal article entitled *"Multiscale exposure to mercury emitted from vegetation during Australian fires"*.

Chapter 3: Field Measurements at Malaysian Peat Fires

3.1 Purpose

Tropical peat fires cause episodes of extremely poor air quality in many parts of Asia, with frequent occurrences studied in the literature [*Hu et al.*, 2018]. Despite the significant negative environmental impacts caused by these fires, assessment of these effects has been hindered greatly due to a lack of characterisation of the smoke composition, especially for fine particle emissions (i.e. $PM_{2.5}$). The primary campaign of this Masters research project was to measure emissions and determine emission factors of $PM_{2.5}$ from peat fires in the outlying provinces of Kuala Lumpur, Malaysia. This chapter will describe how sampling was conducted in the field during the campaign in July to August 2016. It will also present evidence that the emissions of fine particles decrease rapidly with the age of peat fires, and hence introduce the motivation for the laboratory tests presented in Chapter 4: 2017 Malaysian Laboratory Sample Burns.

Figure 21 Example of sample inlets. Left silver cap: Nephelometer, Right blue cap: DustTrak, Centre blue filter line: Model 48i CO, Black units around base of DustTrak inlet: Personal CO monitors.

The schedule for this campaign was highly weather dependent, and with the effects of El Nino in motion, I decided to run the fieldwork on an "on call" basis. Thomas Smith from Kings College London (at the time based in Kuala Lumpur) and Catherine Yule from Monash University, Bandar Sunway, Malaysia campus, provided details on current weather and fire conditions, to provide a basis for ideal times to schedule fieldwork. After a number of small peat fires were discovered burning in the region, my supervisor and I flew to Malaysia on 11th July 2016. The fieldwork took place from Tuesday 12th of July 2016 until Saturday 14th of August, during which time seven full days of sampling were conducted in the Northern end of Selangor, Malaysia, east of Sungai Besar and north of a protected peat forest (Sungai Dusun). Most of the in-situ instruments used in the campaign were on loan from the Office of Environment and Heritage, Atmospheric Science Unit, Lidcombe. The instruments were calibrated the week prior to leaving.

Figure 22 Instrumentation setup; Centre MIDAC FTS provided by Kings College London, Rear right in-situ instrumentation.

Approval for use on an active fire ground was provided for the following set of instruments:

1. A *DustTrak-DRX Aerosol Monitor 8533*,
2. An *Ecotech Aurora 1000G Integrating Nephelometer* and,
3. A *Thermo Scientific Model 48i CO analyser*.

Additional electrochemical CO personal exposure monitors were deployed by UOW to provide supplementary measurements of CO. A MIDAC OP-FTS provided by Kings College London (and operated by Dr. Thomas E.L. Smith) was used to determine the emission factors for CO.

The in-situ instruments were co-located along the downwind edge of burning peat fields. Sample inlets were setup as close to one another as possible, so as to sample similar contents of the smoke plumes (Figure 21), and at a short distance away from the fire to ensure better mixing and homogeneity of sampled smoke. Special care was taken to ensure that no nearby smouldering sources of burning surface material were sampled so that the burning fuel sampled was predominantly peat, Figure 22.

The *MSA Altair Pro CO Single Gas Detectors* provided additional measurements of CO to supplement the CO analyser on the first day of sampling, before they were adversely affected by the humidity of the tropics. The Nephelometer was run to provide validation of PM levels measured by the DustTrak and showed a high correlation across all sampling sites and days. High correlation was also seen between the CO analyser and the DustTrak.

3.2 Malaysian Field Site Descriptions

For each field site a description is provided below including: an explanation of the instrumentation deployed; any issues encountered; solutions to these issues; a description of the weather and a description of the burn and smoke profiles. A satellite image showing the location of the sites is given in Figure 23. A peat core sample of 1570cm^3 was taken from all sites except Site 1, which had a smaller volume sample of 785cm^3 taken. These samples were stored at Monash University, Sunway Bangsar campus, for bulk density determination to be done during the 2017 laboratory campaign.

Malaysian Site Map

Figure 23 shows the site locations relative to each other and the surrounding landscape. In the bottom right-hand corner (southeast of sampling locations), the protected peat swap can be seen and along the top (north) of the image some local Kampungs (villages) can be seen. All sites sampled are on the left-hand side and were all within the same plantation, while background sampling was conducted in a separate part of the plantation network on the right-hand or eastern side of the map, away from immediate influence of any fires.

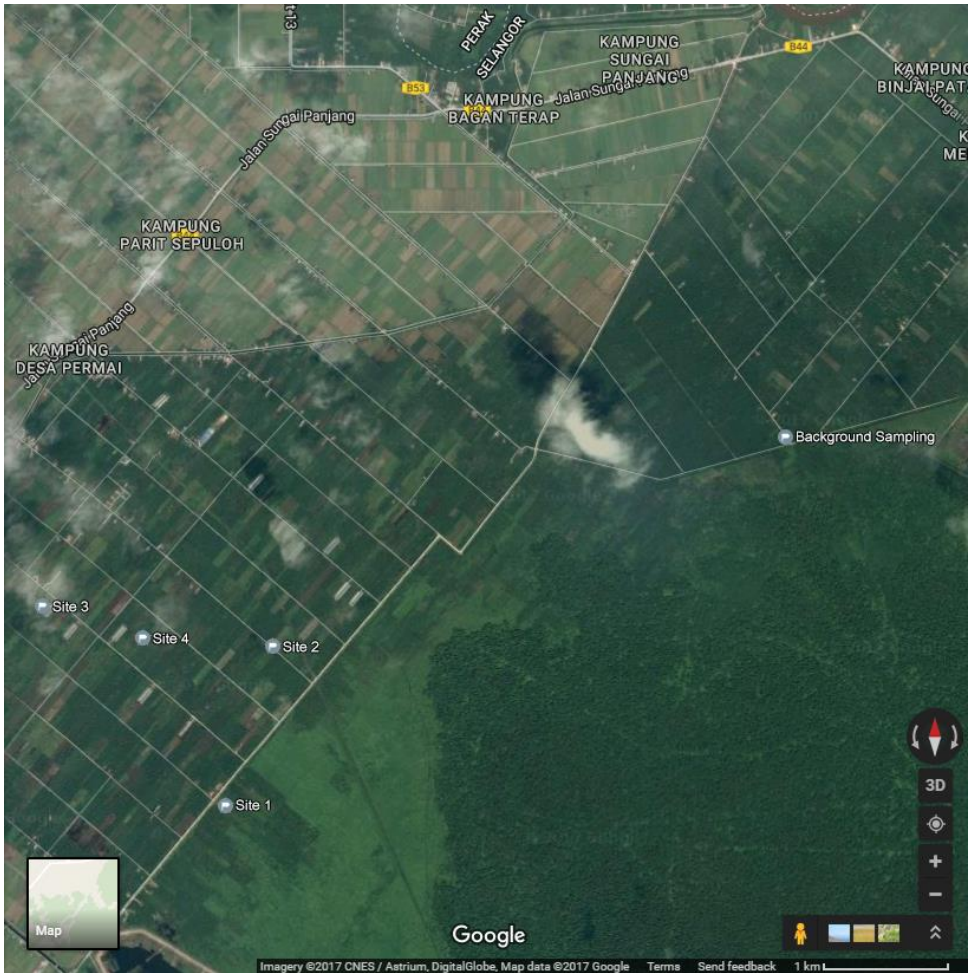

Figure 23 Map of sampling sites. Site 1 to 4 can be seen on the left hand side and the background sampling site can be seen centre right. (Google Maps 2017).

12/07/2016 – Site 1 (3.6752°N, 101.0606°E)

Site 1 was a peat fire that had been started as a result of a "slash and burn", which is a process wherein farmers cut down palm oil palm trees and ignite the remains. This is commonly done to remove basal stem rot disease, which is a soil based fungal infection caused by *Ganoderma boninense*. Burning is the primary solution to this infection due to fungicides being ineffective as a result of degradation in the soil and the cost of fungicides [*Susanto et al.*, 2005]. These slash and burns are often ignited in vacant plots and are generally allowed to burn until completion (i.e. they are extinguished naturally).

Figure 24 Site 1 instrumentation setup.

This burn consisted of turned mounds of peat, approximately five meters deep, which were smouldering, and although palm tree husks were also present on the surface of the peat, there was no visible smoke emanating from them. The ignition date for this burn is unknown, but due to previous reconnaissance was known to have been burning a minimum ten days prior to sampling. Sample inlets were not closely co-located at the site, Figure 24, which led to poorer correlation ($R^2 \approx 0.5$) between CO and $PM_{2.5}$ from this fire than at later fires (when I had refined our experimental set-up). On the left-hand side of the image in Figure 24, the *Model 48i CO Analyser*, DustTrak and personal exposure monitors can be seen. Central is the nephelometer with the *Model 48i CO Analyser's* inlet co-located to the nephelometer's inlet. In the foreground left is the generator, which is running downwind and foreground right is the MIDAC FTIR, which during sampling was relocated to the opposite side of the burn. Figure 25 shows the site layout of Site 1, centre of the image is the MIDAC OP-FTIR directed towards the left-hand side of the screen, where the source was located. Off the left-hand side of the image is the in-situ equipment shown in Figure 24.

Figure 25 Site 1 layout: central is the MIDAC OP-FTIR and to the left (off screen) is in-situ instrumentation and OP-FTIR source.

13/07/2016 – Site 2 (3.6867°N, 101.0640°E)

Site 2 was an okra (ladyfinger) crop that was being prepared for planting. The peat had been ploughed into mounds and ignited at the surface of each mound in preparation for planting (see Figure 26). Our discussions with local environmental groups showed that they did not believe this to be a widespread practice and I was not able to ascertain the reasoning behind this site's appearance and burn pattern. The smoke from this burn was very dense, although the volume of burning peat was much lower. Sampling was conducted halfway down the field from the road (~50m) and approximately 1.5m downwind of the nearest smouldering mound. Instrumentation had much better collocation at this site. As can be seen in Figure 26 and Figure 27 the site is burning in patches, producing a number of individual smoke plumes. Due to the nature of these individual spot fires, the resulting smoke plumes were less homogenous than at other sites, therefore (despite better colocation of sample inlets) the correlation between CO and $PM_{2.5}$ was comparable to Site 1 ($R^2 \approx 0.5$).

Figure 26 Site 2 showing the spot burns observed on the okra. White ash can be seen in the base of the burnt out hole..

Figure 27 Location for instrumentation setup relative to Okra burn. This was the initial setup used to measure combustion efficiency, due to the high levels of smoke PM masks were wore and exposure time minimised when possible.

14/07/2016 – Site 3 (3.6896°N, 101.0473°E)

Site 3 was discovered burning on 02/07/2016, but was not sampled due to the high levels of palm wood and root also burning. Allowing several days of smouldering, permitted the palm material to burn down to husks, which were not readily combustible under the conditions (i.e. the heat from the burning peat was not high enough). No visible signs of burning (i.e. smoke and radiant heat) could be seen from the surface of non-peat material on the 14/07/2016. This site provided much better mixing of smoke than Site 2 and with optimised inlet positioning, there was a much higher correlation between CO and $PM_{2.5}$ ($R^2 \approx 0.9$). Instrumentation was set up ≈75m into the field from the roadside and approximately 5m downwind from the nearest smouldering source. Figure 28 (left-hand image) shows the slash and burn, with the burning peat extending over a greater length than that of sites 1 and 2. The burn was approximately 5m across and the remainder of the field was left cleared. On the right-hand side of this image was a trench that had been dug as a dumping ground, revealing that the water table had fallen at least 3m below the surface of the peat. The right-hand image shows the instrument setup and shows the good colocation of instrument inlets deployed at this burn site.

Due to the lack of shade at the site, the nephelometer was above the standard operation temperature range. Overheating resulted in a failure of the solenoid responsible for the zero measurement. These nephelometer readings were bias approximately 25% lower relative to the DustTrak $PM_{2.5}$ data using the relationship derived at the Werribee smoke chamber experiment (using wood smoke). This was not recognised as an issue until sampling was conducted on the 20th of July 2017 at Site 4, due to the nephelometer not storing over temperature error flags within its dataset.

Figure 28 Site 3 slash and burn. Left hand side is a photograph of the burn and right hand side is an image of the instrumentation setup.

20/07/2016 – Site 4 (3.6875°N, 101.0547°E)

Site 4 was another peat fire that had been ignited as a result of slash and burn practices in the palm oil industry. This was a site where old oil palms with fungal infections were uprooted and brought to be burnt. The palm fronds were ignited and permitted to burn through to the peat soil, and this burn was allowed to continue. The peat swamp (like many in this plantation) had been previously drained, providing a more readily combustible soil base. After six days of burning (in a similar manner to Site 3), I ascertained that any remaining palm material was either non-combustible residue or the heat from the peat smouldering was below ignition temperature. A random spot test and inspection of every large stump and husk, provided confidence that there were no significant emissions from burning surface fuels. Sampling was conducted at the south western end of the field, approximately halfway down the 38m path length of the MIDAC OP-FTIR. The smoke was well mixed and inlets effectively collocated, providing a good correlation ($R^2 \approx 0.8$)(see Figure 29).

The nephelometer had repeated shutter failures and results did not correlate well with the DustTrak. Further investigation revealed that this was an effect of overheating of the nephelometer (as previously mentioned in the 14th of July 2016 Site 3 description). On subsequent hot days, a palm frond hut was built to reduce this effect as shown in Figure 30.

Figure 29 Site 4 sampling setup. Centre front is the MIDAC OP-FTIR operated by the laptop and powered by the orange 12v car battery), centre back are the in-situ instruments, approximately halfway along the FTIR's open path.

27/07/2016 – Site 4 (3.6873°N, 101.0546°E)

Site 4 was sampled again one week after the initial measurements were made. The peat fire remained similar, with the exception of the depth of the burn. The fire had progressed downward, leaving a layer of ash above the smouldering layer. Sampling occurred across the southern length of the burn and field due to a wind shift, but the same area of peat burning was measured again. This plume was well mixed, with adequate sample inlet colocation, thereby providing a high degree of correlation between the $PM_{2.5}$ and CO measurements ($R^2 \approx 0.9$).

Due to the clear sky, there was an increase in sunlight and ambient heat. This, coupled with the lack of shade caused the Nephelometer to reach above its ambient temperature range of 0-40°C, as previously observed on the 20/07/2016. To counter this problem, a palm frond hut was constructed to reduce direct sunlight, whilst still providing adequate airflow for cooling (see Figure 30). This overheating only affected the nephelometer results, since the *Model 48i CO Analyser* and DustTrak both have larger operating temperature ranges. A wide angle view of the burn is shown in Figure 31.

Figure 30 Palm frond huts purpose built to shade instruments on 20/07/2016.

Figure 31 Site 4 day two of sampling (27/07/2016).

03/08/2016 – Site 4 (3.6873°N, 101.0546°E)

The final day of field sampling was once again at Site 4. During the week prior to this sampling, another slash and burn had been prepared on the south-eastern side of the field. In order to ensure that the original peat fire was sampled (that had been burning for 20 days) and not the fresh slash and burn, some modifications to the instrument set-up were made. Sampling was conducted approximately half a meter above the ash layer, with the DustTrak mounted to a tripod and the *Model 48i CO Analyser* run through an extended inlet tube. Figure 32 shows the installation of the DustTrak just above the surface of the ash layer. The *Model 48i CO Analyser* can be seen in the background, under a palm frond hut, and its extended inlet can be seen reaching to the DustTrak's inlet. As can be seen there is faint smoke (not as visibly thick as previous burns) in my immediate vicinity, which was primarily caused by disturbance of the surface when the instruments were set up. This was accounted for during the initial fifteen minutes of warm up period, after which the ash seemed to have settled again. This burn had progressed noticeably deeper beneath the surface of the ash layer than previously sampled burns. (The burn depth was approximately 25cm depth in the areas that I could walk on and deeper in other sections that I did not enter, but rather measured the depth with a stick). These additional deep spots are caused by changes in peat composition and the direction of the flame front. Due to safety considerations, despite the amount of protection provided by my "Magnum structural rated" fire boots, I did not venture further than the side of the burning peat.

Figure 32 Site 4 special sampling setup. The foreground shows me setting up the DustTrak and in the rear the *Model 48i CO Analyser* can be seen under palm fronds and the inlet reaching to the DustTrak inlet.

As can be seen in Figure 33, during sampling on this day, a second slash and burn was ignited on the southern side. Throughout the sampling period, wind direction and speed were also erratic and at times (despite the close proximity of sample inlets to the nearby source), smoke from this new burn reached the sampling instruments. These times were recorded from direct observations and the corresponding measurements were removed from the dataset. The correlation of the CO and $PM_{2.5}$ data from this set is very low ($R^2 \approx 0.1$), primarily due to the low spread of $PM_{2.5}$ and CO concentrations measured and the low number of data points.

Figure 33 Site 4 final sampling day (03/08/2016). Left hand side is the original burn, with the new burn on the right-hand side.

3.3 Modified Combustion Efficiencies & Emission Factors for CO

Modified Combustion Efficiency (MCE) is the measure of how effectively a fire is burning, and is measured by the comparing the ratio of CO_2 emitted versus the sum of CO_2 and CO emitted. This provides an avenue to compare one fire to another. The measurements of MCE used throughout the 2016 field campaign were primarily conducted using a KANE CO_2 and CO analyser deployed by Thomas E. L Smith from Kings College London, England. The KANE 100-1 measures CO_2 and CO by pumping an air sample through a particulate filter and into a cell, which has an electrochemical sensor to measure CO and a non-dispersive infrared sensor to measure CO_2 (just as described Chapter 2, for the MSA Altair Pro Single Gas Detector). The MCE is the ratio of excess CO_2 divided by the excess CO, (where excess is defined as the amount of a gas above the background measurements). The alternative method used to measure MCE during this campaign was with a MIDAC Open-Path Fourier Transform Spectrometer (OP-FTIR). The MIDAC OP-FTIR utilises an infrared source powered by a twelve-volt battery, this source is placed approximately twenty meters away, to create an open path such that the smoke is blown across by the wind. This infrared radiation produced by the source is attenuated at various wavelengths as specific molecules absorb it. The FTIR detector measures this attenuation and can determine the mole fraction of a wide range of carbonaceous species including CO_2, CO, CH_4, C_2H_2, C_2H_4, C_2H_6, H_2CO, CH_3OH, HCOOH and CH_3COOH. Whilst this is not a complete representation of all carbon-containing species emitted by fires, they account of a vast majority (~>98%), such that the emission factor of CO may be determined via Equations 1 and 2 (or via Equations 3 and 4). The EF for CO determined by the MIDAC OP-FTIR on the 20/07/2016 was 205 $g.kg^{-1}$ (205g of CO per kg of peat burnt) and on the 27/07/2016 was 204.5$g.kg^{-1}$. Since the OP-FTIR measures both CO and CO_2, it can also be used to determine the MCE.

Table 2 Modified Combustion Efficiencies from 2016 field.

Date	Site	KANE MCE	FTIR MCE from linear regression
12/07/2016	1	0.84 ± 0.02	
13/07/2016	2	0.81 ± 0.02	
14/07/2016	3	0.85 ± 0.02	
20/07/2016	4	0.84 ± 0.02	0.85 ± 0.02
27/07/2016	4	0.85 ± 0.02	0.85 ± 0.02
03/07/2016	4	0.80 ± 0.02	

Table 2 shows the MCE determined by the Kane-100 and OP-FTS at each of the peat fires where the instruments were deployed. Notice how the combustion efficiency varies very little between different sites and that the difference between MCE determined using the FTIR compared to the KANE 100-1 falls within the standard deviation of each measurement. As can be seen the MIDAC FTIR was only successfully deployed on two sampling days. This is primarily due to an over voltage that occurred during the initial sampling on the 12/07/2016. Once this occurred, the FITR had two error LEDs lit up internally. After contacting MIDAC regarding the error two replacement circuit boards (power and processing boards) where expressed shipped to Malaysia. After arrival of the replacement boards, the entire FTIR unit was disassembled and damaged circuit boards were replaced. Once reassembled the issue was rectified allowing the FTIR to be deployed at appropriate future sampling dates, shown by the line of green lights in Figure 34.

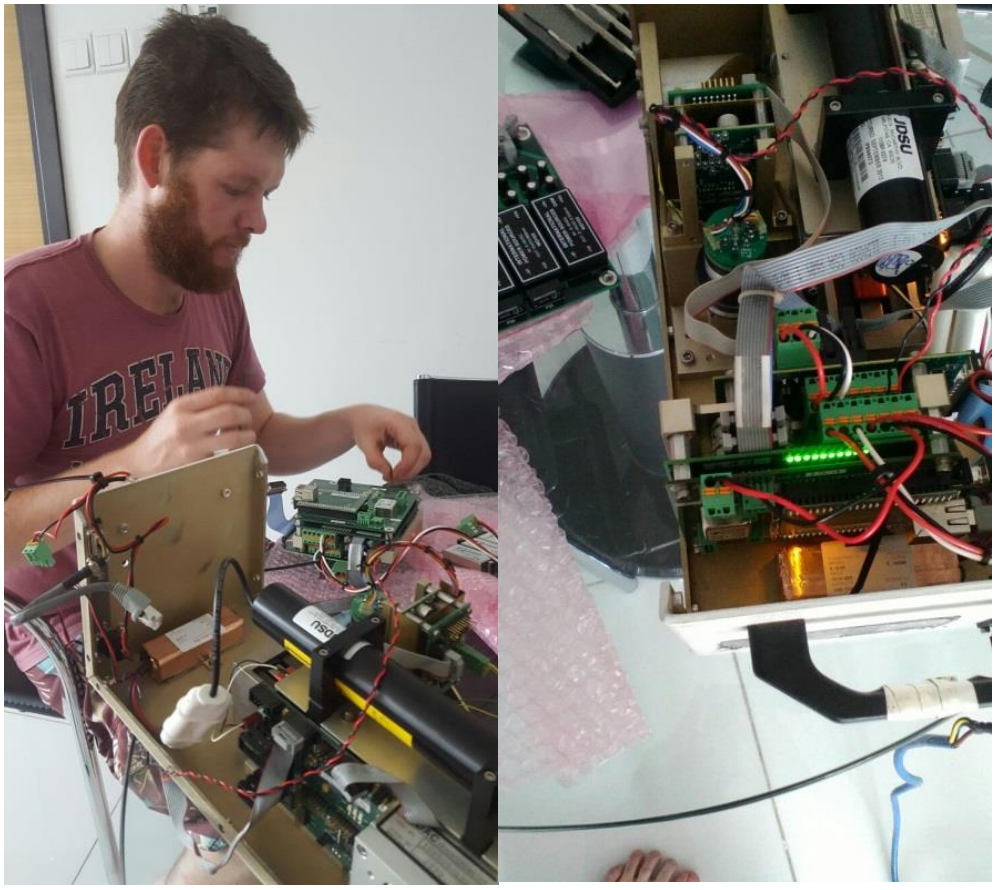

Figure 34 Left: Disassembly and testing of original damaged circuit boards, Right: Post replacement of power and processing printed circuit boards shows all green LEDs with no red or yellow warning lights.

3.4 Malaysian Field Study Results

$PM_{2.5}$ Emission Ratios and Emission Factors

The Emission Factor (EF) for CO was determined using the MIDAC OP-FTIR as described above. Once the MCE for CO was shown to be consistent across not only the KANE 100-1 and the MIDAC OP-FTIR but also across all sites sampled, the EF of 194g of CO per kg of peat burnt was determined to be our best estimate for all fires. An emission ratio between CO and $PM_{2.5}$ was determined by comparing the concentrations measured by the *Model 48i CO Analyser* and the DustTrak. As mentioned in Chapter 1, emission ratios can be determined through various methods [*Paton-Walsh et al.*, 2014]. The two methods employed were:

1. the summation method (where the total excess $PM_{2.5}$ is divided by the total excess CO) and;
2. Using the gradient of the line produced by plotting the concentration of $PM_{2.5}$ against the concentration of CO.

Using the gradient of the linear regression can prove reliable if the relationship shows a high correlation, like the field samples from the 14/07/2016, 20/07/2016 and 27/07/2016. On days where this relationship is not shown to be as strong, the summation method provides a consistent emission ratio, as it correctly weights each measured value by the proportion of total excess carbonaceous species, with the only requirement to be an accurate knowledge of the background mole fractions, which were determined on multiple days to be consistent.

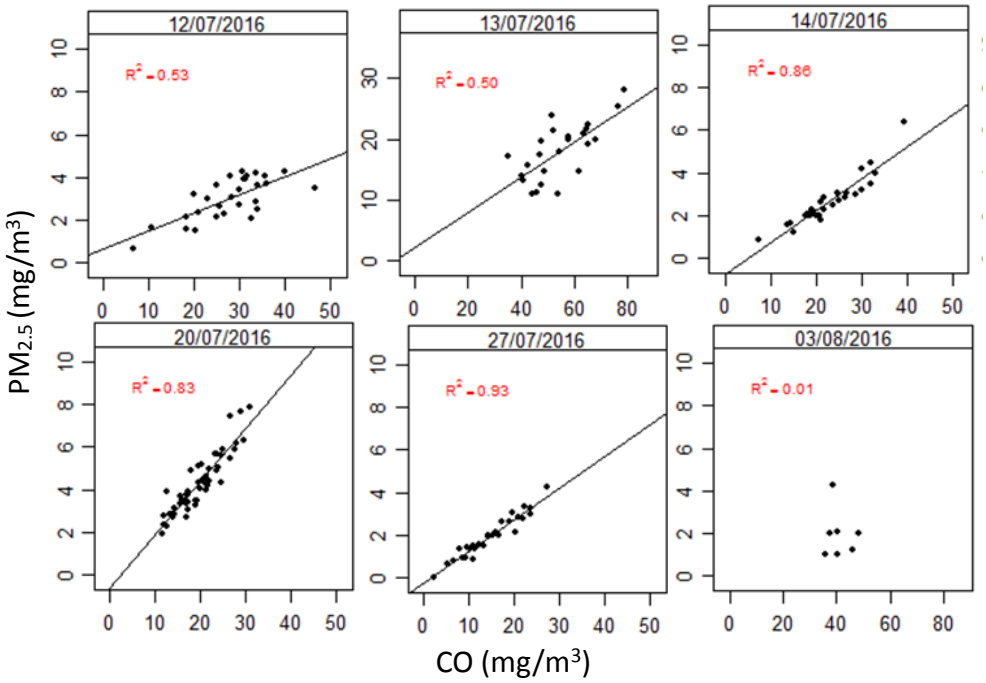

Figure 35 $PM_{2.5}$ vs CO emission ratio across all six field sites. Starting from top left to bottom right shows temporally: Adapted from [*Roulston et al.*, 2018].

The correlation between DustTrak $PM_{2.5}$ and *Model 48i CO Analyser* CO measurements in the time-adjusted series is shown in Figure 35 above. All values shown here have been converted to mg/m^3, which entailed assuming standard pressure and temperature within the *Model 48i CO Analyser* cell. The additional uncertainty from this assumption, is insignificant compared to the large uncertainty (± 20%) assumed in the DustTrak $PM_{2.5}$ concentration measurement. As shown the R^2 value obtained from the relationship is high for the 14th ($R^2 \approx 0.9$), 20th ($R^2 \approx 0.8$) and 27th ($R^2 \approx 0.9$) of July 2016. The causes for reduction in correlation on the 12th and 13th of July 2016 and the 3rd of August 2016 have been detailed above in the site descriptions. The summation method can account for temporary biases caused by the sample ports from the instruments sampling different density of smoke due to non-homogeneity in the plumes. Hence, for the sake of consistency the summation method was elected for use across all sites.

Finally, emission factors for $PM_{2.5}$ were calculated via Equation 12 (which follows the generic form of Equation 5 explained in Chapter 1)

$$EF_{PM2.5} = \frac{\Delta PM_{2.5}}{\Delta CO} \times EF_{CO}$$

Equation 12 Emission factor of $PM_{2.5}$ determined using emission factor of CO

Uncertainties in the emission factor are estimated to be 25% from uncertainties combined in quadrature of 20% from the emission ratio of $PM_{2.5}$/CO and 16% for the emission factor of CO.

A complete summary of the final values from the 2016 Malaysian fieldwork is provided in Table 3. This summary is arranged by age of the burn in approximate days. The sampling date and location provides the site number (additional details can be read above in the site descriptions). MCE is shown to vary very little across all sites. The emission ratio between $PM_{2.5}$ and CO is seen to decrease with time from the ignition of the peat fire. The only anomaly in this trend is seen on the 27th of July 2016, this anomaly falls within the uncertainty of the results and will also be further investigated and explained in Chapter 4. As the emission factor is a directly proportional to the emission ratio (see Chapter 1, Equation 5), the emission factor follows the same pattern as the emissions ratio results.

Table 3 Summary table of Malaysian field sampled Emission Ratios and Emission Factors.

Age of burn (~days)	Sampling Date and Location	MCE	Emission Ratio $PM_{2.5}/CO$	Emission Factor $PM_{2.5}$ $g.kg^{-1}$
0	13/07/2016 Site 2	0.81	0.30 ± 0.06	19 ± 5
6	20/07/2016 Site 4	0.84	0.20 ± 0.04	58 ± 15
>10	12/07/2016 Site 1	0.84	0.10 ± 0.02	20 ± 5
12	14/07/2016 Site 3	0.85	0.10 ± 0.02	38 ± 10
13	27/07/2016 Site 4	0.85	0.12 ± 0.02	23 ± 6
20	03/08/2016 Site 4	0.80	0.04 ± 0.03	8 ± 6

Figure 36 shows how the emission ratio between $PM_{2.5}$ and CO varies with the age of the peat fire and that the MCE varies very little. The top portion of the graph shows a strong anti-correlation between the emission ratio of $PM_{2.5}$ to CO with the age of the peat burn. The red line shows a linear relationship between age of the burn and the emission ratio of CO and $PM_{2.5}$, the blue line shows an exponential fit to these emissions. Both regression methods yield the same correlation ($R^2 \approx 0.97$), although given the physical parameters and the length these burns may last the exponential fit provides a better explanation, since it is expected emissions will continue for the length of the burn. The exponential decay is equivalent to a 9% per day decrease.

The lower panel of Figure 36 shows the MCE and its stability across the fires sampled. It also shows that changes observed in MCE appears to have little to no effect on the emission ratio, this is shown by the lowest two values occurring at either end of the range of emission ratio results.

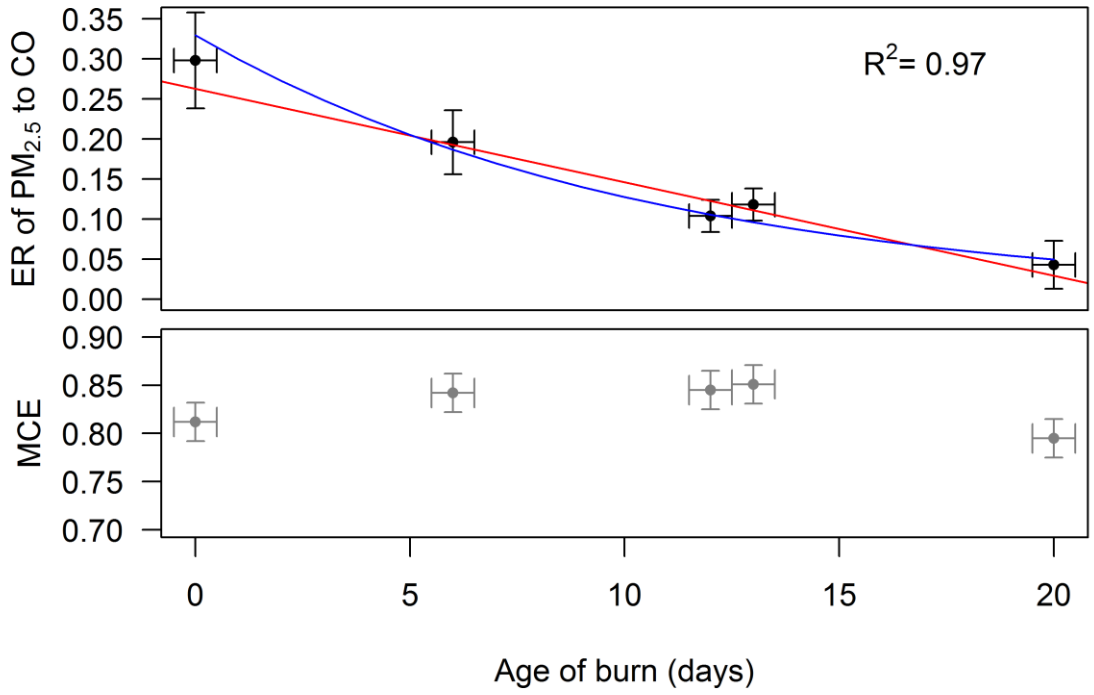

Figure 36 Emission Ratios of $PM_{2.5}$ to CO (upper panel), and MCE (lower panel) as a function of age of burn in days. A liner fit is shown in red and an exponential fit is shown in blue, both yielding an R^2 of 0.97. Error bars indicate estimated uncertainty in age of the burn (± 12 hours); and MCE (± 3%). [*Roulston et al.*, 2018].

Based on observations at the site and the presence of the above trend during a discussion with Dr. Thomas E. L. Smith he suggested a correlation between age emission ratios, together we hypothesised that due to the low intensity smoulder of peat fires, ash that would otherwise be lofted away from the surface of the burn remains and generates an ash layer. From this conversation I designed the laboratory tests detailed in the next chapter. This ash layer traps a percentage of the PM emitted during the burn, the amount trapped increases with the depth of the generated ash layer, causing older fires to adsorb more PM into this layer, preventing it from being emitted.

The emission factors that I derived for newly ignited fires are several times larger than estimates currently used in emissions inventories such as GFED [*Van der Werf et al.*, 2017], meaning that fresh fires may be many times more hazardous than previously estimated. However, since the emissions decrease rapidly, applying a single unchanging emission factor may overestimate PM released when burns last multiple weeks.

Nephelometer Results

The EcoTech Aurora 1000G Nephelometer provided by the OEH Lidcombe was used during the field campaign to provide additional confidence in the validity the TSI DustTrak DRX 8533. This was done by co-locating the inlets and comparing the results from the nephelometer to the $PM_{2.5}$ measured by the DustTrak. This was only partially successful, because of the problems of colocation and inhomogeneity of the smoke plumes in the first two burns. Also, at some of the peat fires, the nephelometer overheated and the resulting data was unreliable. Nevertheless, when running within its operational temperature range, the nephelometer results could provide an additional check on the DustTrak performance. Both the nephelometer and DustTrak sampling caps are not size selective, rather are installed to prevent rain, very large particles and insects from entering the sample lines. Although there is no direct conversion factor between Mm^{-1} and $PM_{2.5}$ concentration, there is a strong correlation between results. This correlation was also shown in Chapter 2 during the Werribee smoke chamber experiment. The nephelometer only makes an actual measurement for fifteen seconds of every minute and hence the sampling of the smoke between the instruments is not equivalent. The best correlation was determined by trailing different averaging times. Site 1 yields the best correlation using two-minute averages, whilst the other fires (at which the nephelometer functioned correctly) yielded the best correlation between DustTrak and nephelometer when using five-minute averages.

To account for differences in sampling times across the instrumentation used and the inaccuracies of instrument internal clocks; I developed an R-script to determine the highest correlation between data points. This script was used across all Malaysia data sets and worked by shifting the data by varying times (adding or subtracting to the time stamp) and comparing the correlation between the data sets.

Once the optimal correlation was determined between the DustTrak and nephelometer relationship, the nephelometer readings at the peat fires were converted to an equivalent $PM_{2.5}$ measurement and then to an emission factor for $PM_{2.5}$ following Equation 12.

Table 4 shows the emission factors calculated using different available measurements and methods of calculation. There are differences between emission factors determined using the gradient of the linear regression and the summation method but these are well within the estimated uncertainty. When correlation of the linear regression between $PM_{2.5}$ and CO is high such as observed on the 14th, 20th and 27th of July 2016 the estimation of the $PM_{2.5}$ emission factor is high by between 25% and 10%. When the correlation is lower, the 12th and 13th the linear regression under estimates compared to the summation. On the 3rd of August 2016 no linear regression could be determined for the site as explained above in the site descriptions.

Table 4 Summary of Emission Factors of PM2.5 determined using different measurements and methods of calculation.

Sampling Date	Age of burn (days)	EF from DustTrak Summation Method (g/kg)	EF from linear regression of DustTrak vs CO (g/kg)	R^2 for CO vs DustTrak	EF from nephelometer Summation Method (g/kg)
20160712	>10	**19 ± 5**	15 ± 4	0.53	(14 ± 4)
20160713	0	**58 ± 15**	51 ± 13	0.5	(49 ± 15)
20160714	12	**20 ± 5**	26 ± 7	0.86	19 ± 6
20160720	6	**38 ± 10**	44 ± 11	0.84	30 ± 9
20160727	13	**23 ± 6**	26 ± 7	0.93	22 ± 7
20160803 Complete	20	12 ± 8	10 ± 3	0.11	
20160803 no wood	20	**8 ± 6**	-	0.012	

The uncertainty applied to the nephelometer was determined by the measurements obtained during the Werribee smoke chamber (Chapter 1) and set at an encompassing value of 30% the measurement to ensure all sources of error where accounted for. During the 12th and 13th of July 2016 (shown in bracket) the comparison is not as strong, this is due to inadequate co-location on the 12th of July 2016 and the low homogeneity of the smoke plumes experienced on the 13th as described above in the site descriptions. The day shown in red on the 20th of July 2016 is as explained above the day where the instrument was operating above the standard operating conditions for the nephelometer, and as such provided unreliable data. The remaining two days that were sampled with good collocation, well mixed homogenous smoke and ran within the standard operating conditions of the nephelometer provide a very close agreement to the DustTrak results once converted from visibility to $PM_{2.5}$ using the conversion factor determined at the Werribee smoke chamber. Both days provide a 95% agreement with the nephelometer measuring ~5% lower that the DustTrak in both instances.

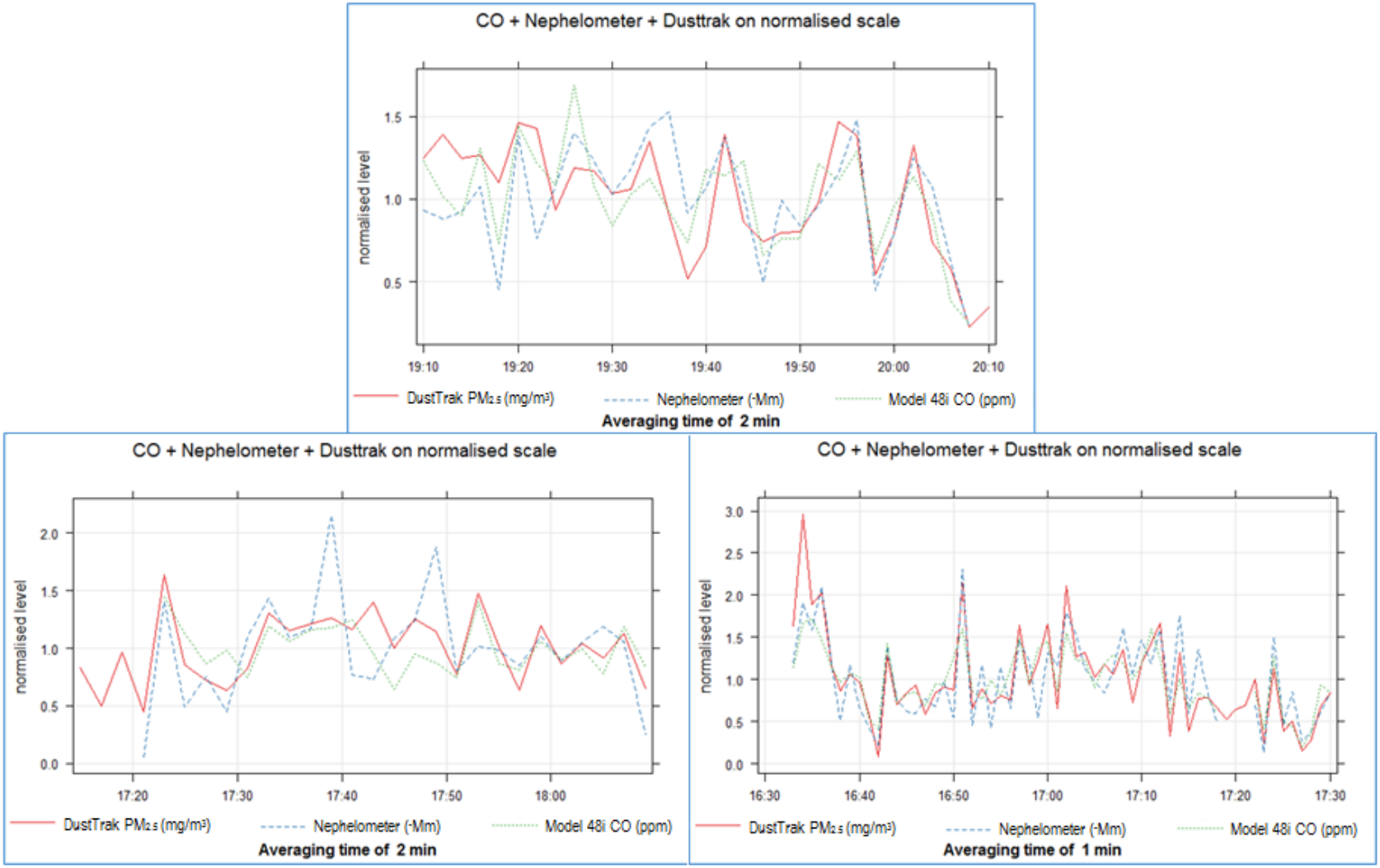

Figure 37 Top: Normalised time series of *Model 48i CO Analyser*, nephelometer and DustTrak results for 12th July 2016, Bottom-Left: Normalised time series of 13th July 2016, Bottom-Right: Normalised time series of 27th July 2016.

3.5 Malaysian Field Campaign 2016 conclusion

The results obtained during the 2016 Malaysian field campaign, suggested a previously unidentified geophysical process. Using the *DustTrak-DRX 8533 Desktop Aerosol Monitor* and the *Thermo Fisher Model 48i Gas Filter Correlation CO Analyser* an emission factor for $PM_{2.5}$ was determined at four peat fires on six separate days.

Our confidence of validity of these results was strengthened by the prior calibration against gravimetric samples in the Werribee study (Chapter 2), the determination of MCE by *MIDAC OP-FTIR* and *KANE 100-1 CO_2/CO analyser* and the use of an *Aurora 1000G integrating Nephelometer* as a check for the *DustTrak* response during the days each instrument was running correctly. Rather than determining the average of a single emission factor, I observed a decreasing emission factor with age of the burn. This relationship provides some insight into the range of $PM_{2.5}$ emission factors observed in other studies [*Stockwell et al.*, 2016].

I hypothesised that as the peat fire progresses, an ash layer builds up on the surface of the peat and acts as a filter of fine PM, thereby reducing emissions to the atmosphere.

The novelty of this finding prompted an investigation of the feasibility of conducting an additional in-depth laboratory study to test this hypothesis. This additional study was conducted from the 1st of January 2017 until the 12th of February 2017 and is detailed in Chapter 4 of this thesis.

Chapter 4: 2017 Malaysian Laboratory Sample Burns

4.1 Purpose

This campaign was designed to test the hypothesis that the emission factor of $PM_{2.5}$ decreases with the age of the peat burn, and that this is due to the accumulation of ash on the surface of the burn. Conducting these additional tests in Malaysia was a product of the availability of peat samples and the strict biosecurity rules employed by Australian border control.

Once ignited, peatlands burn for a long period of time relative to forest fires, with a low energy smoulder the main combustion mode [*Rein*, 2013]. This low energy smoulder provides enough energy to continue the burning process through lower layers of biomass fuel, but not enough convective forces to remove the ash, as is evident in more fierce burns. As shown in Figure 38 the burn progressively consumes fuel, leaving a layer of ash [*Rein et al.*, 2009]. This ash layer might act as a filter for the fine PM thereby explaining the reduction in $PM_{2.5}$ as a function of burn age.

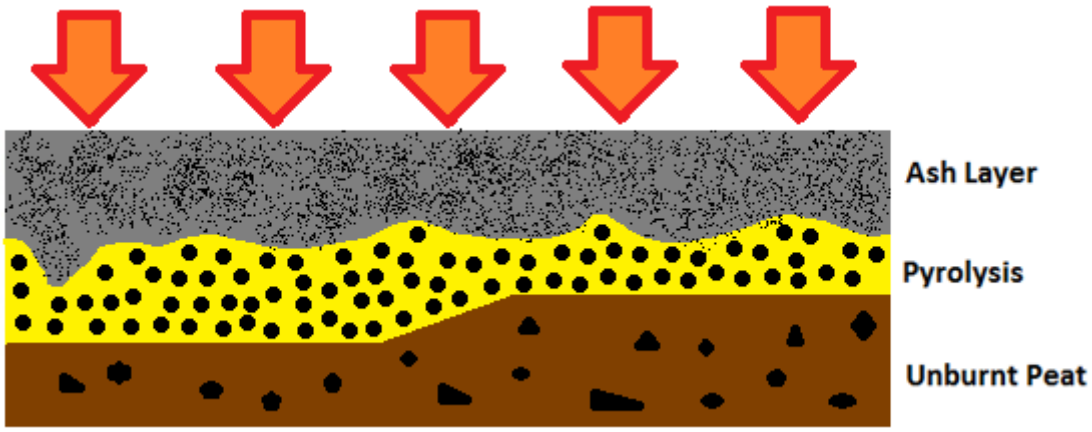

Figure 38 Transect of a natural peat burn. The ash layer is irregular due to differences in fuel and surface topography.

This second campaign was designed to test this theory and ran from the 1st of January 2017 until the 4th of February 2017 in Kuala Lumpur, Malaysia. If my hypothesis was correct, then I would expect a decrease in the emission ratio of $PM_{2.5}$ to CO as the laboratory peat fires progressed and the ash layer is formed on the surface. Additionally, if the ash layer acts as a filter for the $PM_{2.5}$ (which will be predominantly composed of black carbon), then I would expect the carbon content of the ash layer to increase as the burn progressed.

4.2 Planning and preparation

Two burn boxes were sourced by Thomas E. L. Smith from Kings College London prior to conduction the laboratory burns. A new lightweight burn box Figure 39 was commissioned from the *Haze Lab,* Imperial College, London. It was made from a light weight fiber board which is fire proof. The new box measured internal dimensions length 200mm, width 200mm and depth of 100mm, referred to hence forth as the "*new box"*. The second burn box was an older design made from cinder blocks and had internal dimensions of length 170mm, width 130mm and depth of 300mm, and will be referred to as the "*big box"*. The big box was badly damaged on arrival and originally thought to be unsuitable for further testing. Using aluminum flashing, large cable ties and strong tape, I was able to repair the burn box prior to testing as indicated in Figure 40 and Figure 41.

Figure 39 New burn box created by the *Haze Lab,* Imperial College, London.

Figure 40 Big box internal repairs.

Figure 41 Big box external repairs.

The repairs applied to the big box not only fixed the damage but also allowed for easier clean-up and resetting between burns. Given the deeper profile, the big box was primarily used across all tests after initial testing.

Prior to leaving Australia, I designed a smoke sampling hood (using Computer Aided Design tools) that would capture the smoke and provide adequate mixing before the sampling location for the instruments. The smoke hood needed the ability to be flat- packed. Once the design was blueprinted *Wollongong Sheet Metal* undertook the sourcing, primary cutting and bending of the 5mm stainless steel. After receiving the cut and bent steel, a day was spent finalising the initial construction of the hood (see Figure 43). This was completed with the assistance of Aaron Williams and Mervyn Roulston (see Figure 42). Due to some miss communication the exhaust from the fume hood was incorrectly shaped, and required to be re cut and sized to provide the desired effect Figure 46.

After initial construction, a sample burn was conducted on a barbeque hot plate to test the hood could draw smoke towards the sampling location (see Figure 44 and Figure 45). Final construction in Malaysia used pop rivets to create a strong and more permanent construction with less hazardous sharp edges and screws.

Figure 43 Initial preparations for remote construction of smoke hood in the field.

Figure 42 Left Aaron Williams, Right Mervyn Roulston assisting with the drilling of holes for construction rivets.

Figure 46 Sizing and constructing sample hood.

Figure 45 Live fire test of sample hood.

Figure 44 Live smoke test of sample hood showing flow of smoke.

4.3 Laboratory setup and preparation

The burns completed in this campaign used peat sourced from near the 2016 Site 3 (3.6896°N, 101.0473°E), and was obtained in bulk on the 1st of January 2017 by Dr. Thomas Smith and Oliva Pang using a shovel, a large plastic bin and additional plastic containers for storage. An additional sample was taken in a plastic container to be used for bulk density and moisture measurements. Initial test burns were conducted with wet peat in the new burn box, but these required very high intial energy input to ignite. The second batch of test burns were conducted using peat which had been dried using a low temperature stove top (Figure 47) and an oven on low temperature (60°C). The initial oven used at Dr. Catherine Yule's residence had an electrical failure, resulting in the use of laboratory drying ovens at Monash University Kuala Lumpur campus, Sunway Bangsar, Malaysia. All measured burns used in this thesis and the associated journal paper were dried using the laboratory drying oven for a minimum of three days at 60-70°C. This created an absolute dry base, which increased the ignition probability [*Frandsen*, 1997] and encouraged pyrolysis [*Rein et al.*, 2009].

Figure 47 Dr. Clare Murphy slowly heating peat on the stovetop to dehydrate it prior to lab burns.

The laboratory was setup in Dr. Catherine Yule's backyard in the suburb of Taman Tun Abdul Razak, Malaysia. As with the previous field campaign, weather conditions were recorded using a *Kestrel 3500 weather meter*, which consistently showed humidity of above 85%. The data from this meter corrupted during the backup process, such that additional information is no longer available. The humidity provided challenges over the course of test burns, including the effect on ignition of peat and the excess humidity within power points causing some power cuts. One issue (as mentioned previously) was the shorting of the oven, which caused testing to be suspended for a day as the problem was traced to the shorting of a power board.

The laboratory was setup to provide easy access to all instrument panels and so that the distance from the instruments to the sampling point in the smoke hood was minimised. The sample hood pictured in Figure 48 has temporary legs; these were replaced with a permanent set before official testing began.

Figure 49 Construction of the sample hood.

Sample inlets were collocated inside the sample hood. The two gravimetric samplers were located opposite sides of the DustTrak's and CO analyser's inlets. The rear most (closest to the smoke) sample line was labelled *Inlet I* and was attached to MicroVol pump 10-0776. The second inlet closest to the exit of the sample hood was labelled *Inlet II* and was attached to MicroVol pump 08-1015. Both *Inlet II* and MicroVol 08-1015 were visually marked with striped electrical tape to provide an easily recognisable visual cue to which pairs went together for consistency. Results from these gravimetric tests were unexpected, with irregular final weights. This is indicative that there may have been leaks in the system, causing incorrect volumes of smoke to be sampled. All weighing of filters used for gravimetric testing was provided by the Office of Environment and Heritage, Lidcombe, NSW, and conducted by Vilma Silva and Dan Chen from the Chemical Forensics Quality Assurance unit.

Figure 48 Laboratory setup, Left is laptop controlling FTIR, Right is sample hood with burning peat in the bottom right hand corner, under sample hood is DustTrak and in the rear is the Thermo Fisher CO analyser and two MicroVol pumps.

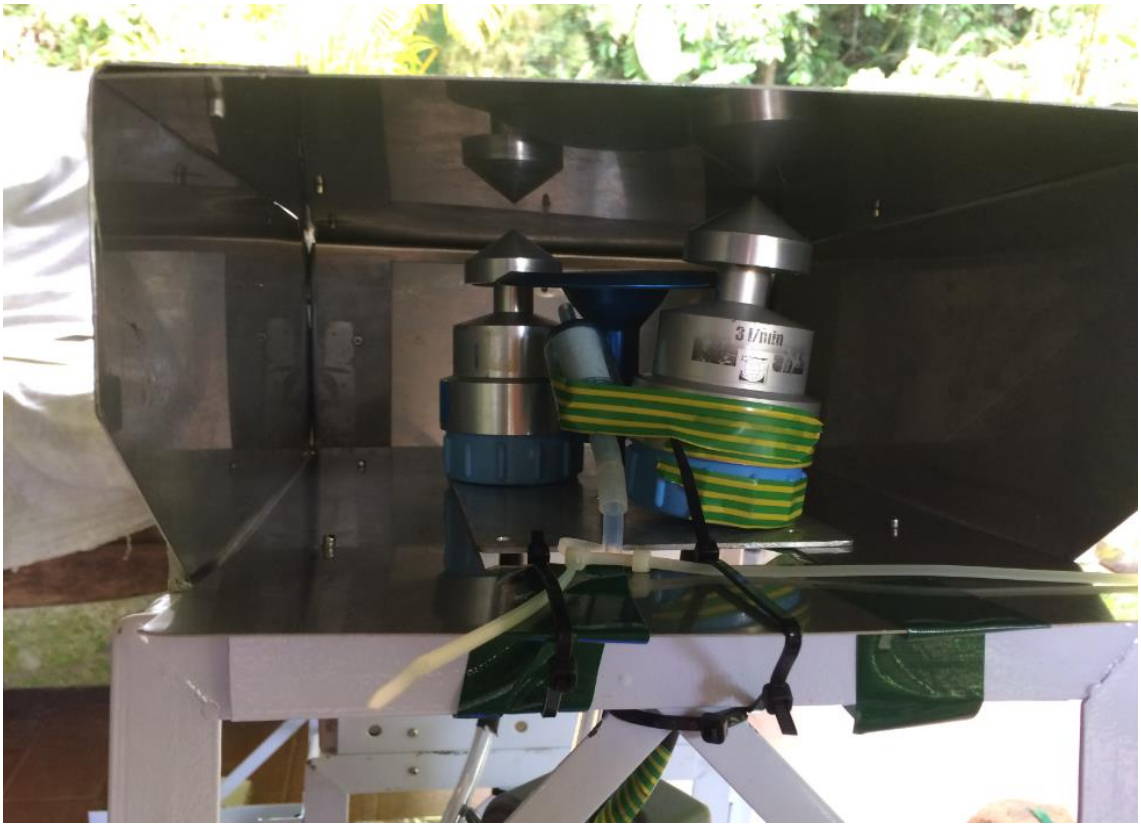

Figure 50 Sample inlets installed above burning peat.

During these laboratory tests I followed the method employed by *Wilson et al. 2015*. In their study a 220x120x100mm insulated burn chamber was filled with *Irish Sphagnum* moss peat. This chamber (similar to our burn box), replicated natural surface combustion, providing insulation and limiting oxygen exchange from the base and sides, leaving only one surface of the peat exposed to open air. This methodology was suggested by *Rein et al. 2009,* as a being an effective approximation to natural burns. The surface was then ignited using a coiled nichrome wire, heated to ~600°C and placed in contact with the surface of the peat. This simulates natural ignition conditions, such as from a surface shrub fire [*Rein et al.*, 2009; *Wilson et al.*, 2015]. Our methodology expanded upon this by using a ceramic plate to disperse the ignition heat to a larger area, providing a wider ignition base, (see Figure 51). This created a more even burn profile. Additionally, it introduced a higher amount of energy in a shorter time to the peat's surface. We used two ignition patterns, which will be discussed during each burn they were deployed at.

Figure 51 Ceramic ignition plate being powered to initiate the laboratory burn. As can be seen the centre and top end of the burn box has already been ignited, this image was taken during step three of the three-phase ignition.

Like the 2016 field campaign Thomas E. L. Smith from Kings College London, England, provided a MIDAC Open-Path FTIR. The key difference to running this instrument in a laboratory setting is the requirement of a white cell. The white cell allows an infrared source to be shone in through an inlet, reflected between very accurately angled mirrors before leaving the cell and reflecting into the MIDAC FTIR detector. After unpacking the white cell and during initial testing it was discovered that the mirrors had become misaligned during shipping, and fogging of the glass and window had occurred due to the high humidity.

4.4 Malaysian Laboratory Results

Peat Bulk Density and Mositure Content

As mentioned in Chapter 3, peat samples were obtained from all sites and stored in air tight containers, for later analysis of the bulk density and moisture content of the fuel. Samples were taken using a core sampler with a measured volume of 785cm^3. The core sampler was a pipe of constant diameter, with a handle and cutting edge to minimise the pressure exerted on the peat ensuring a consistent volume of peat was sampled in each core sample. The bulk density and fuel moisture were determined using standard laboratory techniques. All samples were then weighed using a *Sartorius TE212* balance (calibration date 17/08/2016) and separated into oven trays to facilitate drying. The oven used was a *Memmert UFB 400* (see Figure 52), which was set to 60°C and samples were left for seven days, to ensure complete drying occurred. After drying, the samples were cooled to room temperature for two hours before being re-weighed. Bulk density is calculated as initial weight divided by volume; and fuel moisture is determined as the difference between wet and dry weight.

Figure 52 Memmert UFB 400 drying oven filled with peat samples being dried for bulk density and moisture calculations.

Table 5 shows the summary of percentage moisture and bulk density as determined by the methods described above, for both the July 2016 and January 2017 Malaysian campaigns. Bulk density varies very little across all sites, except Site 2. Site 2 was the okra plantation and the lower density is likely a direct effect of the tilling in preparation for planting. The percentage moisture is also uniform, except for the laboratory burns sample. This was collected during the wet season and at 77% moisture did not ignite readily so was dried prior to burning (as described above). Despite the relatively small variations across the July 2016 sites, a factor of more than six was observed between the largest and smallest emissions ratios of $PM_{2.5}$ to CO, whilst the MCE was relatively constant (~0.83±0.02). It is very unlikely these minor differences in moisture and bulk density explain the variability in emissions of $PM_{2.5}$.

Table 5 Summary of Moisture and Bulk density measurements of peat from July 2016 and January 2017 Malaysian campaigns.

Moisture + Bulk Density Summary		
Sample	Percentage Moisture (%)	Bulk Density (g/cm^3)
2017 Site 3 (Laboratory)	77	0.617
2016 Site 3	53	0.605
2016 Site 4	54	0.625
2016 Site 1	54	0.583
2016 Site 2	62	0.438

Laboratory Burn MCE values

Due to the damage caused to the white cell, FTIR measurements could not be taken for the laboratory burns in January 2017. Due to this, the KANE 100-1 CO_2/CO analyser was required to take all MCE measurements. During the July/August 2016 campaign, I validated the KANE analyser against the MIDAC FTIR and the two instruments showed good agreement. In total six hundred MCE data points, were taken across all laboratory burns and at various stages of the burns. The MCE was determined by measuring CO_2 and CO background concentrations, followed by CO_2 and CO concentrations in the smoke, then averaging each sampling period and using Equation 7 (Chapter 1).

The mean of the MCE measurements is very similar to that of the 2016 field campaign, providing an average MCE across all stages of ~0.83±0.02. Knowledge of the stability of the MCE and the lack of correlation between the small variations with $EF_{PM2.5}$ implies that MCE does not explain the variations in $PM_{2.5}$ seen throughout this campaign. The R^2 values quoted in Table 6 denotes variation between measurements taken by the *KANE 100-1 CO_2/CO analyser*. The high R^2 values displayed here suggest that sampling of MCE was representative of the concentrations being emitted. Uncertainty in the measurements is driven by the 3% uncertainty of the CO electrochemical cell used in the *KANE 100-1 CO_2/CO analyser*.

Table 6 Summary table of MCE from laboratory burns as determined by KANE 100-1 CO_2/CO analyser.

Lab Burns MCE						
Data	**Date**	**Time**	**Notes**	**Burn**	**MCE**	**R^2**
151-190	5-Jan	16:00	After ignition Burn 1	1	**0.83±0.02**	0.74
191-220	6-Jan	12:56	Next day	1	**0.84±0.02**	0.71
221-250	7-Jan	10:00	End of burn 1	1	**0.85±0.02**	0.74
251-080	7-Jan	13:00	After ignition Burn 2	2	**0.85±0.02**	0.76
081-120	8-Jan	17:30	Next day	2	**0.85±0.02**	0.72
121-160	8-Jan	17:45	After scraping	2	**0.85±0.02**	0.63
161-190	9-Jan	12:00	End of burn 2	2	**0.85±0.02**	0.81
191-220	9-Jan	14:00	Burn 3 start	3	**0.87±0.02**	0.68
221-250	9-Jan	15:00	Before ash addition	3	**0.84±0.02**	0.62
251-030	9-Jan	15:20	After ash addition	3	**0.84±0.02**	0.83
031-061	9-Jan	22:00	2200	3	**0.85±0.02**	0.88
062-090	10-Jan	13:00	1300	3	**0.82±0.02**	0.84
091-120	11-Jan	11:00	End of burn 3	3	**0.87±0.02**	0.83
121-150	11-Jan	13:00	New fire Burn 4	4	**0.88±0.02**	0.51
151-180	12-Jan	10:00	Almost all burned	4	**0.86±0.02**	0.86
001-030	12-Jan	12:30	New burn	5	**0.84±0.02**	0.75
031-060	13-Jan	14:45	New burn	6	**0.85±0.02**	0.54
Total			All burn Average	ALL	***0.83*±0.02**	*0.79*

Fire by Fire Analysis of Results

Burn 0 (preliminary testing) - 04/01/2017

The initial test burn undertaken on Wednesday the 4th of January 2017, allowed a number of issues to be identified and sorted out in our operating procedures to ensure consistent methods were employed across all future burns. The initial problems encountered during *Burn 0* included; high fuel moisture, issues with synchronising the gravimetric samplers, inlet co-location and sampling hood setup.

As previously mentioned, after the initial burn, the fuel moisture was controlled by pre-drying all peat prior to burns. The issue with synchronisation of the MicroVol gravimetric samplers was caused by previously configured programmed sample times. This caused one pump to immediately start sampling when power was provided to the pump, while the second pump required manual starting of the run sequence. For consistency, both pump scheduled operation end times were adjusted to a past date, and each instrument manually started for each future sample run. Only 1 hour of data was recorded for the purpose of determining gravimetric results, but due to the moisture of the fuel, the fire was not self-sustaining and required the igniter to be run continuously. Due to this, the data from the test run '*Burn 0'* is not considered to have value in the context of this study and will not be provided or further studied here.

It was also discovered that the CO analyser had developed an issue with its zero value, resulting in low and background concentrations displaying small negative numbers. After returning to Australia and discussing with the OEH Lidcombe staff it was determined that this zero offset was due to a leak in the system near the zero cell. The effect of this zero offset is small at the large concentrations measured values; this effect was determined to be minor and was encompassed by the uncertainty attributed to the measurements.

Burn 1 (First official burn) – 05/01/2017 till 07/01/2017

The burn on the 5th January 2017 was the first burn with useable results and as such is labelled as Burn 1, both here and in the published work [*Roulston et al.*, 2018]. The ignition pattern used for this burn will be called the single point ignition (see Figure 54). This ignition pattern consisted of running the *ceramic igniter* in the centre of the dried peat for half an hour at ~600°C (or 20v to approximate 110w). During this burn some testing of instrumentation was conducted while the igniter was powered, but the values were above detection limit for the DustTrak and as such were removed from the dataset.

Figure 53 shows the time series of the emission ratio of PM2.5 to CO on the left-hand axis and MCE on the right-hand axis a. The MCE remains stable at approximately 0.83 at all stages of the burn. For the first hour after ignition there is an increase in the emission ratio and the MCE is slightly lower than later in the burn. After this peak is reached, a steady reduction in the emission ratio is observed until a sudden spike after approximately ten hours. Our supposition is that this peak is caused by a collapse of the ash layer, due to increased burn depth and intensity in the centre of the ash layer. After this peak, the emission ratio again decreases, which I propose is caused by the ash layer regenerating and reducing the emissions of $PM_{2.5}$ to the atmosphere, such that the emission ratio continues to decrease again.

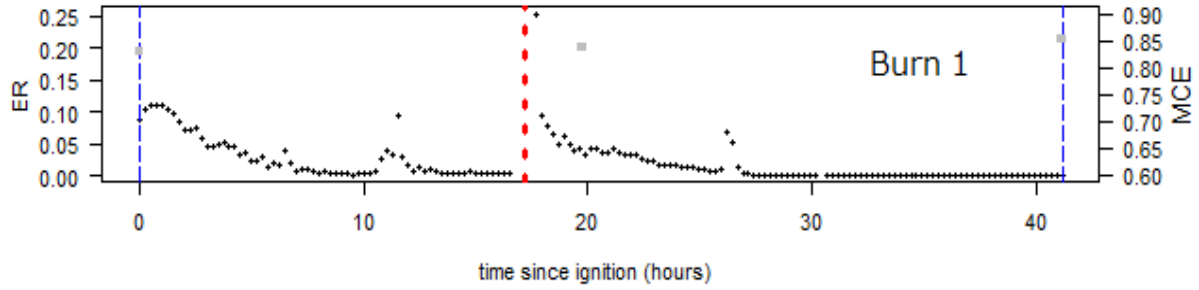

Figure 53 Time-series of 15-minute averages of emission ratios of $PM_{2.5}$ to CO (black-dots and left-hand axis) for Burn 1, The blue line denotes starting time, the red line denotes the ash removal and the grey dots show MCE at various times during the burn.

The red line in Figure 53 denotes the removal of the accumulated ash layer. This was done by carefully removing as much of the ash from the surface whilst leaving the smouldering section as untouched as possible, as shown in Figure 55. This was done primarily to see if removing the ash layer would change the emission ratio of $PM_{2.5}$ to CO. Removing the initial ash layer formed also removes any influence of the ceramic igniter such as the charring of surface peat. As is shown in Figure 53, after the removal of the ash layer there is the largest emission ratio of $PM_{2.5}$ to CO seen during this burn, immediately followed by a very rapid decrease. This peak is likely to result from the combination of the removal of the ash filtering effect and the artificial disturbance of the surface particulates. It could also indicate that emissions are at their highest when the peat is initially ignited at the surface (since at the start of each burn measurements were delayed until the ceramic ignition plate had been removed). Once again, a peak is observed after ten hours of sampling. This phenomenon is seen across multiple burns and the collapse of the ash layer after several hours of burning, is our current hypothesis as to a reason for this.

Figure 55 Removal of ash layer between burns.

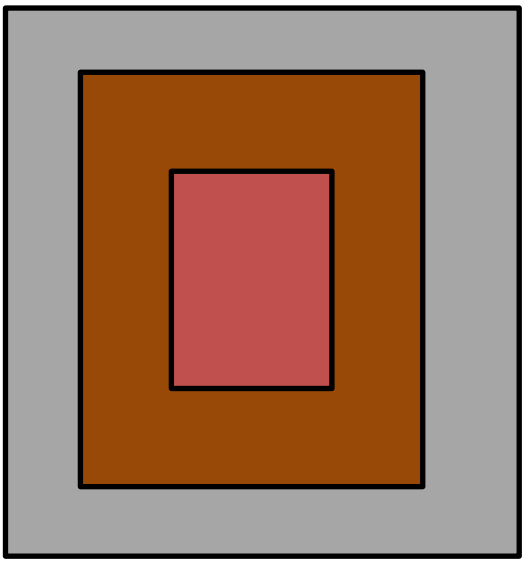

Figure 54, Ignition pattern 1. This image shows and approximation of the single point ignition setup as viewed from above the box. The igniter is shown by red box, the brown box approximates peat and the grey shows the bounds of the burn box.

Burn 2 (Three point ignition pattern used) – 07/01/2017 till 09/01/2017

Burn 2 like burn 1 was conducted in the big burn box. Unlike burn 1, burn 2 used the second ignition pattern (see Figure 56). Ignition pattern 2 used three points of ignition, each for 20 minutes. The goal of this ignition pattern was to avoid the "ash fall" spike in the data that is seen during the previous burns. Unfortunately, the effect of this pattern produced three different depths of burn, each with a progressively deeper ash layer. Figure 57 shows from ignition (0 hours) until approximately fifteen hours into the burn, there is a much greater variability in the emission ratio from one point to the next, than seen in any of the other burns. This is most likely caused by the presence of three burns at various stages and insufficient mixing of the plumes from each. Despite the scatter caused by the alternative ignition pattern, the trend of a reduction in the emission ratio between $PM_{2.5}$ and CO with time since ignition is clearly shown. For eleven hours between 12:06 04/01/2017 until 11:04 05/01/2017, a gap in the data is experienced due to a power outage. As with *Burn 1*, after the removal of the accumulated ash layer (red dotted line on Figure 57), a very large peak in $PM_{2.5}$ to CO emission ratio is visible, coincident with the exposure of the smouldering surface, followed by a reduction to background levels over the following hours. Approximately thirty-four hours after the initial ignition of this burn, or eight hours after the removal of the ash layer a suspected *ash collapse* is observed. Due to the data scatter, and additional ignition time required, which delayed the measurements of emission ratios, *Burn 2* was the only burn to use ignition *Pattern 2*.

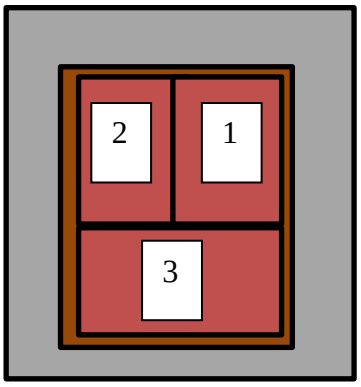

Figure 56, Ignition pattern 2. This ignition pattern used three ignition points each of which ran for 20 minutes. The goal of this ignition pattern was to reduce the effect of the ash collapse witnessed in the previous burn and to create an even depth burn across the entire surface of the peat.

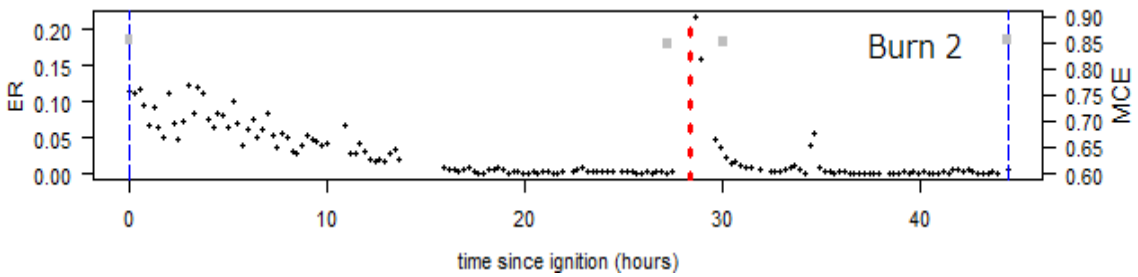

Figure 57 Time-series of 15-minute averages of emission ratios of $PM_{2.5}$ to CO (black-dots and left-hand axis) for Burn 2. The blue line denotes the starting time, the red line denotes the ash removal and the grey dots show MCE at various times during the burn.

Burn 3 (Ash addition experiment) – 09/01/2017 till 11/01/2017

After the completion of *Burn 2* the ash and any remaining peat was removed from the *Big Burn Box* and the box cleaned. Peat that had been freshly dried and allowed to cool at Monash University, Sunway Bangsar, was transferred into the *Big Burn Box* before ignition *Pattern 1* was used to ignite the top layer of ash. After allowing the burn to progress for one-hour post ignition phase, a layer of pre-incinerated ash was placed on top of the smouldering peat. Thomas E. L. Smith generated the ash at Kings College London, London, England, by inserting locally sourced (United Kingdom) Irish sphagnum peat moss into a furnace at 550°C for forty-eight hours. This created artificial ash with extremely low carbon content. The addition of this ash layer was intended to investigate if the ash layer was the cause of the $PM_{2.5}$ emission ratio decrease and that the carbon-rich particulates are being trapped in the ash. The carbon content could be measured both before and after the burn had progressed.

Figure 58 shows the Burn 3 has a similar trend to Burn 1 (Figure 53) where, as the burn progressed the emission ratio between CO and $PM_{2.5}$ steadily decreases until very low levels are observed. During the initial ignition and first twenty hours the ash addition experiment was conducted. The blue line on the left hand side of Figure 58 shows ignition. Forty minutes after ignition the layer of pre-incinerated ash was poured evenly across the surface of the burn. This is shown by the grey line and a sudden step-change decrease in the emission ratio of CO and $PM_{2.5}$ measured. It was also noted that the MCE did not change when the ash layer was added. Subsequently, there was a gradual increase in $PM_{2.5}$ to CO emission ratio. An increasing amount of smoke was visible while I was observing the burn, blackened cracks formed in the ash surface and around the edge of the ash layer, allowing unfiltered smoke to escape. The emission ratio plateaued after approximately 3 hours and a decrease is then seen, once a natural ash layer is generated below the artificially added one. The peak emission ratio observed is lower than in any other burn, due to the ash layer filter catching particulates during the initial peak. After the removal of the of the built up ash layer, designated by the red dotted line in Figure 58, a stabilisation period is observed followed by an decline in particulate emissions, as the ash layer regenerates. This trend is observed across all burns.

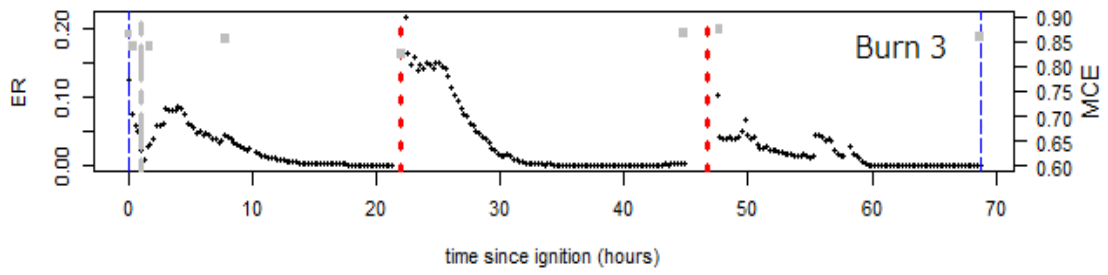

Figure 58 Time-series of 15 minute averages of emission ratios $PM_{2.5}$ to CO (black-dots and left-hand axis) for Burn 3, the blue line denotes starting time, the red line denotes the ash removal and the grey dots show MCE at various times during the burn.

Carbon and Nitrogen percentage in collected ash

Carbon and nitrogen content measurements were taken from ash and peat samples throughout this campaign. The carbon and nitrogen content was tested by Dr Stephanie Evers (from Liverpool John Moores University, Liverpool, UK). The analysis used peat and ash subsamples that were oven dried at 105°C for seven hours and then homogenised by a hand-mill. These subsamples were analysed in 20mg aliquots by a Thermo Flash EA 1112 total element analyser with a detection limit between 100 ppm and 100% content.

Table 7 shows the percentage of carbon and nitrogen in the samples taken at various stages of the burns. Burn 0 (unburnt peat) is a sample of raw peat, which shows just over 50% carbon by weight. Pre-incinerated ash contains very low (~0.6%) carbon content as expected after decomposition. Burn 1 ash (bottom) 06/01/2017 was ash taken from the base of the generated ash layer and has a low carbon content (~1.3%); the sample from the top of Burn 1 sample was contaminated with unburnt peat during sampling due to experimental error. Burn 1 ash (top) 07/01/2017 was taken from the top of the ash layer on the second day of burning and has a notably lower concentration of carbon than the unburnt peat, but more than five times the concentration from the base of the same burn on day 1 (~5.4%). The hypothesis is that this increase in carbon content maybe attributed to the filtering of PM during the burning process: carbonaceous species escape in gaseous form during the combustion reaction, but a proportion of the PM becomes trapped within the channels of the peat through which the smoke travels.

The trend is also observed during Burn 2, where the top of the ash layer (~40% carbon) is more than double that of the base layer (~15% carbon). Both the top and bottom carbon content of this burn are much higher than the values from the previous burn. This could be caused a less complete combustion of the peat. Burn 2 had its top layer sampled on the 08/01/2017, and as this layer was not removed until the 09/01/2017 no base layer sample was taken on the 08/01/2017.

Despite variation in the absolute values measured a trend is observed across these two sampled burns, where the upper layers of ash have an increased concentration of carbon than the lower layers of ash. Greater carbon content in the oldest (highest) layers of ash suggests this may be the sink for particulate carbon that is missing in the emission ratios, i.e. the particulate carbon is trapped in the ash layer rather than escaping into the atmosphere.

Table 7 Measured percentage carbon in ash samples taken during laboratory burns. A trend is seen across all sampled burns, with the concentration at the top of each ash layer being higher than the base of the same burn, showing an accumulation of carbon in the upper layers of the ash layer.

Ash Source	% Carbon
Burn 0 Unburnt peat 05/01/2017	50.45
Pre-incinerated ash	0.58
Burn 1 Ash (Bottom) 06/01/2017	1.32
Burn 1 Ash (Top) 07/01/2017	5.34
Burn 1 Ash (Base) 07/01/2017	2.26
Burn 2 Ash (Top) 08/01/2017	10.47
Burn 2 Ash (Top) 09/01/2017	39.76
Burn 2 Ash (Base) 09/01/2017	14.82

Table 8 shows the percentage carbon content, of the pre-generated ash, unburnt peat and the ash layer at different stages of the ash addition experiment. The starting percentage in the pre-incinerated ash is very low at ~0.6% and additional carbon measured as the burn progresses must arise through contamination, either by carbon depositing from the smoke or from accidental sampling of nearby unburnt peat. To minimise contamination from unburnt peat, samples were carefully removed from the surface of the ash layer. After the first hour a sample was taken from a blackened area of the surface ash and an increased level of carbon was observed in the sampled ash layer, up to ~7%. Then from 110 minutes through to fifteen hours a lower but still inflated carbon content was observed from the ash layer. There is significant variation and I believe that the surface ash was probably highly inhomogeneous due to a large amount of smoke seen escaping around the edges of (and cracks in) the artificial ash layer. The sample from the edge of the ash layer after fifteen hours of burning, shows a large increase in carbon content of nearly 40%; this is attributed to the high concentration of smoke seen escaping around perimeter of the ash layer.

Table 8 Carbon levels in ash addition experiment. An excess of smoke escaped around the edges of the ash layer rather than being filtered, this is displayed with high levels of carbon being observed along these edges.

Start (%)	60min (%)	110min (%)	210min (%)	395min (%)	15hour (%)	15hr edge of ash (%)
0.58	7.38	2.11	1.25	1.06	4.70	38.34

4.5 Summary and Conclusions from the Malaysian Laboratory Burns

The second Malaysian campaign took a multifaceted approach to test the hypothesis that emissions of $PM_{2.5}$ decrease with time since ignition due to a filtering of fine PM by the ash layer that is generated as the burn progresses. These laboratory tests were designed to measure a number of other variables that might also contribute to the variation in emission ratios of $PM_{2.5}$ to CO that were observed during the field campaign. To ensure homogeneity among samples, all peat used in the laboratory burns was sourced from the same peat swamp. The bulk density of peat samples from field campaign sites were determined and shown to be very similar in all sites except site 2, the okra burn.

During the laboratory burns, the MCE was regularly measured and showed little variation across all stages of the burn, despite the variety of emission factors observed. The laboratory burns provided strong corroborating evidence that the variations in emission ratios of $PM_{2.5}$ to CO that was measured during the field campaign were indeed the result of changes as the burn progresses and an ash layer forms. Throughout all burns (other than the ash addition experiment, and during episodes of ash collapse), a trend was observed where the emission ratio between $PM_{2.5}$ and CO decreases with time until very low $PM_{2.5}$ emission ratios are observed or the burn extinguishes.

The results from the ash addition experiment showed that the carbon content of the artificially added ash was very variable, probably due to an excess of smoke escaping around the edges and cracks in the artificial ash layer. Nevertheless, the results still provided convincing evidence to support the ash filtration theory. All ash samples exposed to the burning peat had a greater carbon content than the artificially ash layer added, with a consistently larger carbon content at the surface of the ash layer than measured at the base of the ash layer.

In conclusion, the additional laboratory burns described in this chapter confirmed that the $PM_{2.5}$ emissions decrease as the peat burns progress. Further evidence was obtained from these laboratory burns (and in particular from the ash addition experiment) coupled with the carbon content tests, to support the theory that this decrease in $PM_{2.5}$ emissions is due to the ash layer acting as a filter and capturing a significant portion of the fine PM and preventing its release to the atmosphere.

Chapter 5: Summary and Conclusions

5.1 Overview of Main Conclusions

The initial goal of this thesis was to improve the understanding of particulate emissions from tropical peat fires in Peninsula Malaysia. The work presented in this thesis included an initial campaign to validate instrumentation within a smoke chamber. This was followed by an initial field campaign, where gaseous carbonaceous species (including; CO_2, CO, CH_4, C_2H_2, C_2H_4, C_2H_6, H_2CO, CH_3OH, HCOOH and CH_3COOH) were measured using a MIDAC FTIR to produce an emission factor for CO. This emission factor and the ratio between enhanced $PM_{2.5}$ and CO concentrations was used to determine the emission factor of $PM_{2.5}$. During this initial campaign a trend was discovered, where the age of the peat fire influenced $PM_{2.5}$ emissions, with the emission factor decreasing over time. It was hypothesised that this was due to the generation of a filtering ash layer.

Prompted by a wish to test this hypothesis, a second campaign was designed, adding a new focus, verifying the existence of this ash filter effect. This was conducted with dried peat within a controlled laboratory setting, where ignition, burn size, moisture and bulk density were all controlled. This provided strong evidence that the emission ratio between $PM_{2.5}$ and CO reduced over the age of the burn. The addition of pre-incinerated *Irish Sphagnum peat moss* showed how the carbon content percentage increased, accounting for a percentage of the missing $PM_{2.5}$.

These results have provided a greater understanding of the emissions of tropical peat fires and can provide a basis for further study into emission factors to be implemented across emission inventories used by chemical transport models.

5.2 Outcomes for Specific Aims of the Thesis

Chapter 1 lists specific objectives to be achieved throughout the course of the thesis. These are detailed below in italics and the outcomes are discussed.

1. *To test and validate the instruments to be used in this project within a controlled smoke chamber at the Victoria University Werribee site (As explained in Chapter 2);*

The instrumentation was acquired pre-calibrated on loan from the Office of Environment and Heritage, Lidcombe, NSW. Once initial training was completed the instruments were installed at the Victoria University Werribee site within the smoke chamber. The results from this study showed a high correlation between the TSI *DustTrak-DRX 8533 Desktop Aerosol monitor*, Ecotech *Aurora1000G Integrating Nephelometer* and the Federal Reference Method *Thermo Fisher Partisol 2000i-D Dichotomous Air Sampler* across the three particulate sources (wood smoke, coal smoke and diesel exhaust). The DustTrak also compared well to a real time Federal Equivalent Method *Thermo Fisher Beta Attenuation Monitor 1022*. From this, it was determined that a correction factor for peat smoke was not required for the DustTrak and instead a large uncertainty (± 20%) would be assumed, to account for potential biases caused by differences in the size distribution of the peat and wood smoke particulates.

The *MSA Altair Pro CO Single Gas Detectors* were compared to the *Thermo Fisher Model 48i Gas Filter Correlation CO Analyser* with daily calibrations showed a high agreement providing good correlation, precision and accuracy across all CO sources. The Victorian EPA is currently preparing this work for publishing.

The above work is described in detail in Chapter 2 of this thesis.

2. *To determine particulate ($PM_{2.5}$) emission factors from tropical peat fires in peninsula Malaysia, through in-situ measurements. These were conducted using the following instruments (also validated at the Werribee smoke chamber): an Ecotech Aurora 1000g Integrating Nephelometer, a Thermo-Scientific Model 48i Gas Filter Correlation Carbon Monoxide Analyser, a TSI DustTrak DRX-8533 Desktop Model Aerosol Monitor, and four MSA Altair Pro Single Gas Detectors (As described in Chapter 3);*

A field campaign was conducted in peninsula Malaysia during July and August of 2016, to determine particulate emissions factors from tropical peat fires. This campaign involved sampling four different fires with three repeat sampling periods at *site 4*. During sampling the *Ecotech Aurora 1000G Integrating Nephelometer* was used as a method of validating the *DustTrak DRX-8533*.Using an averaging time of five minutes, a strong correlation was observed across all burns that the nephelometer functioned correctly.

During the initial day of field sampling the *Thermo-Scientific Model 48i Gas Filter Correlation Carbon Monoxide Analyser* and *MSA Altair Pro Single Gas CO Sensors* were compared. This comparison showed a good agreement providing evidence that the instrumentation had not been negatively affected by transport.

An emission ratio between PM less than 2.5 microns (measured by the DustTrak unit) and carbon monoxide (measured by the CO analyser) was determined. An emission factor of 205grams of CO per kilogram of peat burnt, as determined by a *MIDAC Open Path Fourier Transfer Infrared Spectrometer*, was combined with the $PM_{2.5}$ and CO emission ratios to determine an emission factor for $PM_{2.5}$ at each of the sites. This work is detailed in Chapter 3 and the results have been published in the *Journal of Geophysical Research: Atmospheres*:

Fine Particle Emissions From Tropical Peat Fires Decrease Rapidly With Time Since Ignition

The above work is detailed in Chapter 3 of this the thesis.

3. *To obtain measurements of fire fighter exposure to carbon monoxide at hazard reduction burns conducted by the New South Wales Rural Fire Service. These measurements will be made using CO sensors which were validated at the Werribee smoke chamber and will contribute to a study estimating total exposure to a range of toxins (As detailed in Chapter 2);*

The initial study using validated instrumentation from the Werribee smoke chamber was completed. The *MSA Altair Pro Single Gas CO sensors* were deployed at two Hazard Reduction burns, attached the chest of volunteer fire fighters conducting a range of duties and actions in accordance with training and instruction from the fire controllers. The results, are to be combined with a number of similar measurements and published by Katrina Macsween from the University of New South Wales (UNSW). This paper combines CO exposure measurements with measured emission ratios between CO and Hg to estimate potential Hg exposure experienced by volunteer fire fighters at hazard reduction burns. The results are to be published in an article entitled:

Multiscale exposure to mercury emitted from vegetation during Australian fires

The above work is described in detail in Chapter 2 of this thesis.

4. *To undertake laboratory burn studies in Malaysia to verify theories developed from analysis of initial fieldwork about the effect of the ash layer on particulate emissions (As shown in Chapter 4);*

In January 2017, a laboratory study was undertaken in peninsula Malaysia. This study involved the burning of collected peat samples in a burn box, with sampling occurring in a smoke hood. The results provided convincing evidence in favour of the theory that the

generation of an ash layer was the cause of the variability observed in the previous 2016 campaign (Chapter 3). The previously validated DustTrak and model 48i CO analyser showed a strong exponential decrease in the emission ratio between CO and $PM_{2.5}$. Each burn showed at least one artefact, where the emission ratio increased again briefly, which I hypothesised was caused by an ash collapse event, after which a reduction in $PM_{2.5}$ to CO was once again observed. During each burn, the Modified Combustion Efficiency (MCE) was measured repeatedly, to ensure that any change in particulate emissions was not related to a change in the intensity of the burn. The bulk density and moisture of each burn was maintained by the preparation of the peat prior to burning.

The ash addition experiment successfully showed a sudden decrease in the emissions of $PM_{2.5}$ when the ash was added and an increase in carbon content when compared to the pre-incinerated peat ash used to form an artificial layer. This provided compelling evidence that the generated ash layer was filtering the missing PM. A detailed explanation of methods and results is provided in Chapter 4, and the results are in a paper currently in review:

Newly ignited peat fires emit unexpectedly large amounts of fine particles

5.3 Recommendations for future work

There are a number of additional campaigns that could be made to improve the understanding of how particulates are emitted from peat burns and their wider impact on the environment, and local and global populations.

- A more in-depth categorisation of emitted particulates with experiments being conducted within a fume hood setting that would allow for controlled dilution of smoke with particulate free air, providing a better understanding of initial surface emissions without reaching concentrations above the detection limit of instrumentation. This categorisation would be achieved by analysis of collected gravimetric filters;
- Additional field campaigns at landscape scale burns at which an air quality-sampling pod could be installed on a more permanent basis to observe the life of the fire from ignition to the time the fire is extinguished;
- A study into whether a similar ash layer filtering effect occurs in temperate and boreal peat fires, and if yes, to quantify if how pronounced the effect is in these similar fuel sources;
- A comparative study between pollution events in major cities around the world, which could be also compared to known large-scale fires in the local vicinity of these cities, to examine the similarities and differences between air quality both during and after these events. This could then be extrapolated using hospital admittance records to estimate the effect on local populations in these cities;
- Additional research into methods of detecting smaller ignitions and burns that are not observed by the current methods employed (MODIS, etc.), as a number of these burns are never accounted for and as such will be missed from even the most in-depth inventories;
- A laboratory study measuring the emissions from undried peat. This could be conducted by first igniting dried peat in a large sand bed with a large amount of undried peat beneath. This fire would then progress into the undried layer, after which the ash generated from the dried sample would be removed;

5.4 Concluding Comments

The effects of landscape scale tropical peatland fires are wide reaching. They contribute an estimated 10% of total greenhouse gas emissions generated from deforestations and forest degradation [*Ballhorn et al.*, 2009; *Langmann et al.*, 2009], significantly increase premature mortalities [*Koplitz et al.*, 2016] and impact on both human health and regional economies in affected areas [*Gaveau et al.*, 2014]. Due to the long burn times and the long-range transport of emitted pollutants, large areas of the globe are impacted [*Andreae*, 1983; *Edwards et al.*, 2006; *Viatte et al.*, 2015]. Despite these well-documented effects, very little peer reviewed research has been released regarding these emissions. In this study, emission factors for $PM_{2.5}$ from peat fires have been successfully measured. Significantly larger values were found from newly ignited fires than those currently assumed in global fire emissions inventories [*Van der Werf et al.*, 2017]. Additional work is needed to better quantify the best values that should be used in chemical transport models. Nevertheless, this thesis presents evidence for a previously unknown natural phenomenon, whereby emissions of fine particles decrease as the fire progresses due to the filtering effect of the ash layer being generated on the surface. This phenomenon also explains the large variability observed in previous measurements of emission factors for particulates from peat fires.

The research conducted for this thesis has also culminated in the authourship of a paper which has recently been published in the Journal of Geophysical Research: Atmospheres and has such proven that the research stands up to peer-review and has merit in the greater scientific community [*Roulston et al.*, 2018].

Bibliography

Akagi, S. K., R. J. Yokelson, C. Wiedinmyer, M. J. Alvarado, J. S. Reid, T. Karl, J. D. Crounse, and P. O. Wennberg (2011), Emission factors for open and domestic biomass burning for use in atmospheric models, *Atmospheric Chemistry and Physics*, *11*(9), 4039-4072.

Akimoto, H. (2003), Global Air Quality and Pollution, *Science*, *302*(5651), 1716-1719.

Andreae, M. O. (1983), Soot Carbon and Excess Fine Potassium: Long-Range Transport of Combustion-Derived Aerosols, *Science*, *220*(4602), 1148.

Andreae, M. O. (1991), Biomass burning: its history, use, and distribution and its impact on environmental quality and global climate, *Global biomass burning: Atmospheric, climatic and biospheric implications*, 3-21.

Ballhorn, U., F. Siegert, M. Mason, and S. Limin (2009), Derivation of burn scar depths and estimation of carbon emissions with LIDAR in Indonesian peatlands, *Proceedings of the National Academy of Sciences*, *106*(50), 21213-21218.

Beelen, R., O. Raaschou-Nielsen, M. Stafoggia, Z. J. Andersen, G. Weinmayr, B. Hoffmann, K. Wolf, E. Samoli, P. Fischer, and M. Nieuwenhuijsen (2014), Effects of long-term exposure to air pollution on natural-cause mortality: an analysis of 22 European cohorts within the multicentre ESCAPE project, *The Lancet*, *383*(9919), 785-795.

Chameides, W. L., et al. (1999), Case study of the effects of atmospheric aerosols and regional haze on agriculture: An opportunity to enhance crop yields in China through emission controls?, *Proceedings of the National Academy of Sciences*, *96*(24), 13626-13633.

Christian, T. J., B. Kleiss, R. J. Yokelson, R. Holzinger, P. J. Crutzen, W. M. Hao, B. H. Saharjo, and D. E. Ward (2003), Comprehensive laboratory measurements of biomass-burning emissions: 1. Emissions from Indonesian, African, and other fuels, *Journal of Geophysical Research: Atmospheres*, *108*(D23).

Crutzen, P. J., and M. O. Andreae (1990), Biomass burning in the tropics: impact on atmospheric chemistry and biogeochemical cycles, *Science*, *250*(4988), 1669-1678.

Davies, S. J., and L. Unam (1999), Smoke-haze from the 1997 Indonesian forest fires: effects on pollution levels, local climate, atmospheric CO2 concentrations, and tree photosynthesis, *Forest Ecology and Management*, *124*(2–3), 137-144, doi:http://dx.doi.org/10.1016/S0378-1127(99)00060-2.

Ecotech (2009), Auroa 1000 User Manual, edited.

Edwards, D. P., G. Pétron, P. C. Novelli, L. K. Emmons, J. C. Gille, and J. R. Drummond (2006), Southern Hemisphere carbon monoxide interannual variability observed by Terra/Measurement of Pollution in the Troposphere (MOPITT), *Journal of Geophysical Research: Atmospheres*, *111*(D16), n/a-n/a, doi:10.1029/2006JD007079.

Ezzati, M., and D. M. Kammen (2001), Quantifying the effects of exposure to indoor air pollution from biomass combustion on acute respiratory infections in developing countries,

Environmental Health Perspectives, *109*(5), 481-488.

Field, R. D., et al. (2016), Indonesian fire activity and smoke pollution in 2015 show persistent nonlinear sensitivity to El Niño-induced drought, *Proceedings of the National Academy of Sciences*, *113*(33), 9204-9209.

Fishman, J., K. Fakhruzzamen, B. Cros, and D. Nganga (1991), Identification of widespread pollution in the southern hemisphere deduced from satellite analyses, *Science*, *252*, 1693-1696.

Frandsen, W. H. (1997), Ignition probability of organic soils, *Canadian Journal of Forest Research*, *27*(9), 1471-1477.

Gaveau, D. L. A., et al. (2014), Major atmospheric emissions from peat fires in Southeast Asia during non-drought years: evidence from the 2013 Sumatran fires, *Scientific Reports*, *4*, 7, doi:10.1038/srep06112.

Geron, C., and M. Hays (2013), Air emissions from organic soil burning on the coastal plain of North Carolina, *Atmospheric Environment*, *64*, 192-199, doi:http://dx.doi.org/10.1016/j.atmosenv.2012.09.065.

Giglio, L., J. T. Randerson, and G. R. van der Werf (2013), Analysis of daily, monthly, and annual burned area using the fourth-generation global fire emissions database (GFED4), *Journal of Geophysical Research: Biogeosciences*, *118*(1), 317-328, doi:10.1002/jgrg.20042.

Haikerwal, A., F. Reisen, M. R. Sim, M. J. Abramson, C. P. Meyer, F. H. Johnston, and M. Dennekamp (2015), Impact of smoke from prescribed burning: Is it a public health concern?, *Journal of the Air & Waste Management Association*, *65*(5), 592-598, doi:10.1080/10962247.2015.1032445.

Hamada, Y., U. Darung, S. H. Limin, and R. Hatano (2013), Characteristics of fire-generated gas emission observed during a large peatland fire in 2009 at Kalimantan, Indonesia, *Atmospheric environment*, *74*, 177-181.

Hao, W. M., and D. E. Ward (1993), Methane production from global biomass burning, *Journal of Geophysical Research: Atmospheres*, *98*(D11), 20657-20661.

Hooijer, A., S. Page, J. G. Canadell, M. Silvius, J. Kwadijk, H. Wösten, and J. Jauhiainen (2010), Current and future CO2 emissions from drained peatlands in Southeast Asia, *Biogeosciences*, *7*, 1505-1514.

Hu, Y., N. Fernandez-Anez, T. E. L. Smith, and G. Rein (2018), Review of emissions from smouldering peat fires and their contribution to regional haze episodes, *International Journal of Wildland Fire*.

Huijnen, V., M. J. Wooster, J. W. Kaiser, D. L. A. Gaveau, J. Flemming, M. Parrington, A. Inness, D. Murdiyarso, B. Main, and M. van Weele (2016), Fire carbon emissions over maritime southeast Asia in 2015 largest since 1997, *Scientific Reports*, *6*, 26886, doi:10.1038/srep26886.

Jayarathne, T., C. E. Stockwell, A. A. Gilbert, K. A. Daugherty, M. A. Cochrane, K. C. Ryan, E. I. Putra, B. H. Saharjo, A. D. Nurhayati, and I. Albar (2016), Chemical characterization of

fine particulate matter emitted by peat fires in Central Kalimantan, Indonesia during the 2015 El Niño, *Atmos. Chem. Phys. in preparation*.

Johnston, F., I. Hanigan, S. Henderson, G. Morgan, and D. Bowman (2011), Extreme air pollution events from bushfires and dust storms and their association with mortality in Sydney, Australia 1994–2007, *Environmental Research*, *111*(6), 811-816, doi:http://dx.doi.org/10.1016/j.envres.2011.05.007.

Konecny, K., U. Ballhorn, P. Navratil, J. Jubanski, S. E. Page, K. Tansey, A. Hooijer, R. Vernimmen, and F. Siegert (2016), Variable carbon losses from recurrent fires in drained tropical peatlands, *Global Change Biology*, *22*(4), 1469-1480, doi:10.1111/gcb.13186.

Koplitz, S. N., et al. (2016), Public health impacts of the severe haze in Equatorial Asia in September-October 2015: demonstration of a new framework for informing fire management strategies to reduce downwind smoke exposure, *Environ. Res. Lett.*, *11*(9), 10, doi:10.1088/1748-9326/11/9/094023.

Kunii, O., S. Kanagawa, I. Yajima, Y. Hisamatsu, S. Yamamura, T. Amagai, and I. T. S. Ismail (2002), The 1997 Haze Disaster in Indonesia: Its Air Quality and Health Effects, *Archives of Environmental Health: An International Journal*, *57*(1), 16-22, doi:10.1080/00039890209602912.

Kuwata, M., F. M. Kai, L. Yang, M. Itoh, H. Gunawan, and C. F. Harvey (2017), Temperature and burning history affect emissions of greenhouse gases and aerosol particles from tropical peatland fire, *Journal of Geophysical Research: Atmospheres*, *122*(2), 1281-1292.

Langmann, B., B. Duncan, C. Textor, J. Trentmann, and G. R. van der Werf (2009), Vegetation fire emissions and their impact on air pollution and climate, *Atmospheric Environment*, *43*(1), 107-116, doi:http://dx.doi.org/10.1016/j.atmosenv.2008.09.047.

Le Tertre, A., S. Medina, E. Samoli, B. Forsberg, P. Michelozzi, A. Boumghar, J. Vonk, A. Bellini, R. Atkinson, and J. Ayres (2002), Short-term effects of particulate air pollution on cardiovascular diseases in eight European cities, *Journal of epidemiology and community health*, *56*(10), 773-779.

Lelieveld, J., J. S. Evans, M. Fnais, D. Giannadaki, and A. Pozzer (2015), The contribution of outdoor air pollution sources to premature mortality on a global scale, *Nature*, *525*(7569), 367-371.

Levine, J. S., W. R. Cofer, and J. P. Pinto (1993), Biomass Burning, in *Atmospheric Methane: Sources, Sinks, and Role in Global Change*, edited by M. A. K. Khalil, pp. 299-313, Springer Berlin Heidelberg, Berlin, Heidelberg, doi:10.1007/978-3-642-84605-2_14.

Mead, M. I., et al. (2013), The use of electrochemical sensors for monitoring urban air quality in low-cost, high-density networks, *Atmospheric Environment*, *70*, 186-203, doi:http://dx.doi.org/10.1016/j.atmosenv.2012.11.060.

MSA Safety Appliances Company (2011), *MSA Altair Pro Single Gas Detector*, MSA North America, Cranberry Township, Pennsylvania.

NSW (1997), Protection of the environment operations act 1997, edited by N. Government.

NSW (2010), Protection of the Environment Operations (Clean Air) Regulation 2010, in *2010-428*, edited by N. S. W. Government.

NSW OEH (2014), About the air quality index, edited.

Ostro, B., and L. Chestnut (1998), Assessing the Health Benefits of Reducing Particulate Matter Air Pollution in the United States, *Environmental Research*, *76*(2), 94-106, doi:http://dx.doi.org/10.1006/enrs.1997.3799.

Page, S. E., F. Siegert, J. O. Rieley, H.-D. V. Boehm, A. Jaya, and S. Limin (2002), The amount of carbon released from peat and forest fires in Indonesia during 1997, *Nature*, *420*(6911), 61-65.

Paton-Walsh, C., T. E. L. Smith, E. L. Young, D. W. T. Griffith, and É. A. Guérette (2014), New emission factors for Australian vegetation fires measured using open-path Fourier transform infrared spectroscopy – Part 1: Methods and Australian temperate forest fires, *Atmos. Chem. Phys.*, *14*(20), 11313-11333, doi:10.5194/acp-14-11313-2014.

Pedroza, R., LPI, SPOT, AAM, SKM, OEH, Sensis, and Kaltron (2016), Martins Creek Prescribed Burn Incident Action Plan, *Map Projection: GDA 1994 MGA Zone 1956*, RAF Pedroza.

Prockop, L. D., and R. I. Chichkova (2007), Carbon monoxide intoxication: An updated review, *Journal of the Neurological Sciences*, *262*(1–2), 122-130, doi:http://dx.doi.org/10.1016/j.jns.2007.06.037.

Raub, J. A., M. Mathieu-Nolf, N. B. Hampson, and S. R. Thom (2000), Carbon monoxide poisoning — a public health perspective, *Toxicology*, *145*(1), 1-14, doi:http://dx.doi.org/10.1016/S0300-483X(99)00217-6.

Rein, G. (2013), Smouldering fires and natural fuels, in *Fire Phenomena and the Earth System: An Interdisciplinary Guide to Fire Science*, edited, pp. 15-33, doi:https://dx.doi.org/10.1002/9781118529539.ch2.

Rein, G., S. Cohen, and A. Simeoni (2009), Carbon emissions from smouldering peat in shallow and strong fronts, *Proceedings of the Combustion Institute*, *32*(2), 2489-2496.

Reisen, F., and S. K. Brown (2009), Australian firefighters' exposure to air toxics during bushfire burns of autumn 2005 and 2006, *Environment International*, *35*(2), 342-352, doi:http://dx.doi.org/10.1016/j.envint.2008.08.011.

Reisen, F., S. M. Duran, M. Flannigan, C. Elliott, and K. Rideout (2015), Wildfire smoke and public health risk, *International Journal of Wildland Fire*, *24*(8), 1029-1044.

Reisen, F., D. Hansen, and C. P. Meyer (2011), Exposure to bushfire smoke during prescribed burns and wildfires: Firefighters' exposure risks and options, *Environment International*, *37*(2), 314-321, doi:http://dx.doi.org/10.1016/j.envint.2010.09.005.

Rivas, I., et al. (2017), Identification of technical problems affecting performance of DustTrak DRX aerosol monitors, *Science of The Total Environment*, *584*, 849-855,

doi:http://dx.doi.org/10.1016/j.scitotenv.2017.01.129.

Roulston, C. P.-W., C, T. E. L. Smith, É.-A. Guérette, C. M. Yule, G. Rein, and G. R. van der Werf (2018), Fine Particle Emissions From Tropical Peat Fires Decrease Rapidly With Time Since Ignition, *Journal of Geophysical Research: Atmospheres*, doi:https://doi.org/10.1029/2017JD027827.

Rückerl, R., A. Schneider, S. Breitner, J. Cyrys, and A. Peters (2011), Health effects of particulate air pollution: a review of epidemiological evidence, *Inhalation toxicology*, *23*(10), 555-592.

Samet , J. M., F. Dominici , F. C. Curriero , I. Coursac , and S. L. Zeger (2000), Fine Particulate Air Pollution and Mortality in 20 U.S. Cities, 1987–1994, *New England Journal of Medicine*, *343*(24), 1742-1749, doi:doi:10.1056/NEJM200012143432401.

Smith, T. E. L., S. Evers, C. M. Yule, and J. Y. Gan (2017), In situ tropical peatland fire emission factors and their variability, as determined by field measurements in Peninsula Malaysia, *Global Biogeochemical Cycles*.

Stetter, J. R. (2008), Amperometric Gas SensorsA Review, *Chemical reviews*, *108*(2), 352-366, doi:10.1021/cr0681039.

Stewart, R. D. (1975), The effect of carbon monoxide on humans, *Annual review of pharmacology*, *15*(1), 409-423.

Stockwell, C. E., T. Jayarathne, M. A. Cochrane, K. C. Ryan, E. I. Putra, B. H. Saharjo, A. D. Nurhayati, I. Albar, D. R. Blake, and I. J. Simpson (2016), Field measurements of trace gases and aerosols emitted by peat fires in Central Kalimantan, Indonesia, during the 2015 El Niño, *Atmospheric Chemistry and Physics*, *16*(18), 11711-11732.

Stockwell, C. E., R. J. Yokelson, S. M. Kreidenweis, A. L. Robinson, P. J. DeMott, R. C. Sullivan, J. Reardon, K. C. Ryan, D. W. T. Griffith, and L. Stevens (2014), Trace gas emissions from combustion of peat, crop residue, domestic biofuels, grasses, and other fuels: configuration and Fourier transform infrared (FTIR) component of the fourth Fire Lab at Missoula Experiment (FLAME-4), *Atmospheric Chemistry and Physics*, 9727.

Susanto, A., P. S. Sudharto, and R. Y. Purba (2005), Enhancing biological control of basal stem rot disease (Ganoderma boninense) in oil palm plantations, *Mycopathologia*, *159*(1), 153-157.

Thermo Fisher Scientific (2007), Model 48i Instruction Manual, in *Gas Fileter Correlation CO Analyzer*, edited, p. 320, Air Quality Instruments, Franklin, many.

TSI Incorporated (2012), DUSTTRAK™ DRX AEROSOL MONITOR THEORY OF OPERATION.

Turetsky, M. R., B. Benscoter, S. Page, G. Rein, G. R. Van Der Werf, and A. Watts (2015), Global vulnerability of peatlands to fire and carbon loss, *Nature Geoscience*, *8*(1), 11-14.

Van der Werf, G. R., D. C. Morton, R. S. DeFries, J. G. J. Olivier, P. S. Kasibhatla, R. B. Jackson, G. J. Collatz, and J. T. Randerson (2009), CO2 emissions from forest loss, *Nature geoscience*, *2*(11), 737-738.

Van der Werf, G. R., J. T. Randerson, L. Giglio, G. J. Collatz, M. Mu, P. S. Kasibhatla, D. C. Morton, R. S. DeFries, Y. Jin, and T. T. van Leeuwen (2010), Global fire emissions and the contribution of deforestation, savanna, forest, agricultural, and peat fires (1997–2009), *Atmospheric Chemistry and Physics*, *10*(23), 11707-11735, doi:10.5194/acp-10-11707-2010.

Van der Werf, G. R., et al. (2017), Global fire emissions estimates during 1997–2015, *Earth Syst. Sci. Data Discuss.*, *2017*, 1-43, doi:10.5194/essd-2016-62.

Varon, J., P. E. Marik, R. E. Fromm Jr, and A. Gueler (1999), Carbon monoxide poisoning: a review for clinicians, *The Journal of Emergency Medicine*, *17*(1), 87-93, doi:http://dx.doi.org/10.1016/S0736-4679(98)00128-0.

Vedal, S., and S. J. Dutton (2006), Wildfire air pollution and daily mortality in a large urban area, *Environmental Research*, *102*(1), 29-35, doi:http://dx.doi.org/10.1016/j.envres.2006.03.008.

Viatte, C., K. Strong, J. Hannigan, E. Nussbaumer, L. K. Emmons, S. Conway, C. Paton-Walsh, J. Hartley, J. Benmergui, and J. Lin (2015), Identifying fire plumes in the Arctic with tropospheric FTIR measurements and transport models, *Atmospheric Chemistry and Physics*, *15*(5), 2227-2246, doi:10.5194/acp-15-2227-2015.

Ward, D. E., and L. F. Radke (1993), Emissions measurements from vegetation fires: A comparative evaluation of methods and results, *Dahlem Workshop Reports: Environmental Sciences Research Report 13*, *13*.

Wijedasa, L. S. (2016), Peat soil bulk density important for estimation of peatland fire emissions, *Global Change Biology*, *22*(9), 2959-2959, doi:10.1111/gcb.13364.

Wilson, D., S. D. Dixon, R. R. E. Artz, T. E. L. Smith, C. D. Evans, H. J. F. Owen, E. Archer, and F. Renou-Wilson (2015), Derivation of greenhouse gas emission factors for peatlands managed for extraction in the Republic of Ireland and the United Kingdom, *Biogeosciences*, *12*(18), 5291.

Wooster, M. J., P. H. Freeborn, S. Archibald, C. Oppenheimer, G. J. Roberts, T. E. L. Smith, N. Govender, M. Burton, and I. Palumbo (2011), Field determination of biomass burning emission ratios and factors via open-path FTIR spectroscopy and fire radiative power assessment: headfire, backfire and residual smouldering combustion in African savannahs, *Atmos. Chem. Phys.*, *11*(22), 11591-11615, doi:10.5194/acp-11-11591-2011.

Yibarbuk, D., P. J. Whitehead, J. Russell-Smith, D. Jackson, C. Godjuwa, A. Fisher, P. Cooke, D. Choquenot, and D. M. J. S. Bowman (2001), Fire ecology and Aboriginal land management in central Arnhem Land, northern Australia: a tradition of ecosystem management, *Journal of Biogeography*, *28*(3), 325-343, doi:10.1046/j.1365-2699.2001.00555.x.

Yokelson, R. J., T. Karl, P. Artaxo, D. R. Blake, T. J. Christian, D. W. T. Griffith, A. Guenther, and W. M. Hao (2007), The Tropical Forest and Fire Emissions Experiment: overview and airborne fire emission factor measurements, *Atmos. Chem. Phys.*, *7*(19), 5175-5196, doi:10.5194/acp-7-5175-2007.

Yokelson, R. J., R. Susott, D. E. Ward, J. Reardon, and D. W. T. Griffith (1997), Emissions

from smoldering combustion of biomass measured by open-path Fourier transform infrared spectroscopy, *Journal of Geophysical Research: Atmospheres*, *102*(D15), 18865-18877.

Zhang, H., S. Wang, J. Hao, L. Wan, J. Jiang, M. Zhang, H. E. S. Mestl, L. W. H. Alnes, K. Aunan, and A. W. Mellouki (2012), Chemical and size characterization of particles emitted from the burning of coal and wood in rural households in Guizhou, China, *Atmospheric Environment*, *51*, 94-99, doi:https://doi.org/10.1016/j.atmosenv.2012.01.042.